Supporting Information

A Cd(II) and Zn(II) selective naphthyl based [2]rotaxane acts as an exclusive Zn(II) sensor upon further functionalization with pyrene

Somnath Bej, Mandira Nandi and Pradyut Ghosh*

School of Chemical Sciences, Indian Association for the Cultivation of Science, 2A & 2B Raja S. C. Mullick Road, Kolkata 700032, India. E-mail: icpg@iacs.res.in

List of contents

Synthetic Scheme:

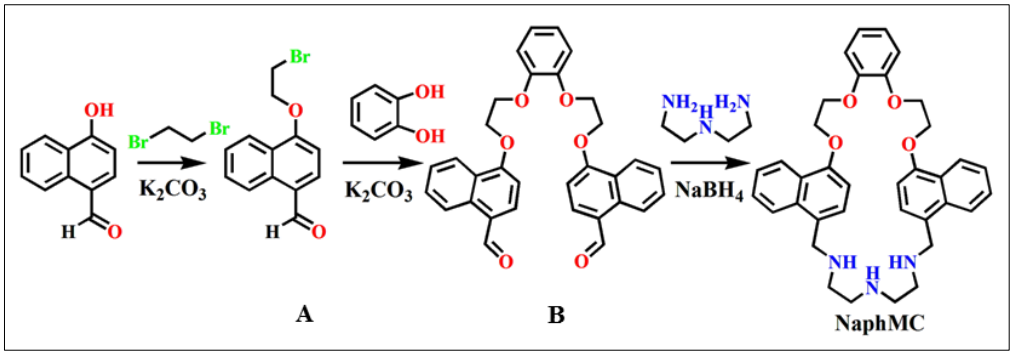

Scheme 1S: Synthetic route of **NaphMC**.[1] Yields: (A: 262 mg, 94%; B: 354 mg, 70%; and NaphMC: 175 mg, 76%).

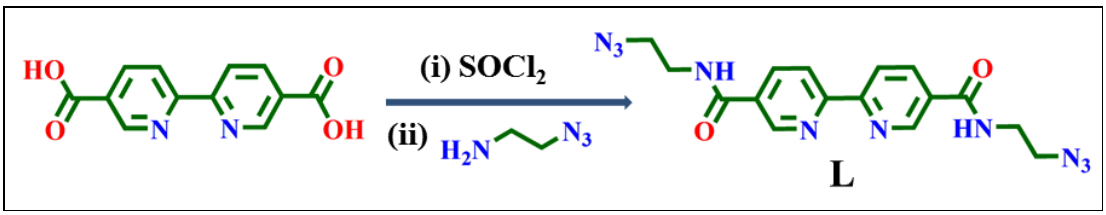

Scheme 2S: Synthetic route of **L**.[2] (Yield: 304 mg, 80%).

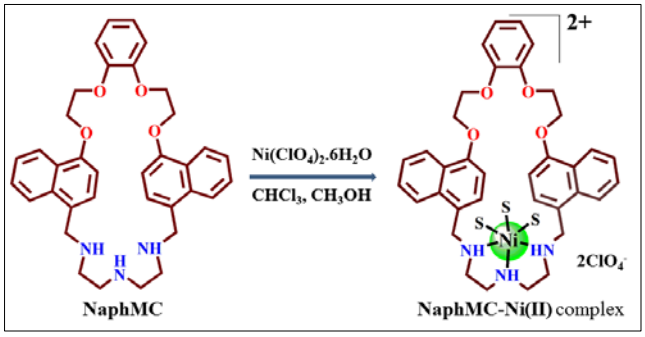

Scheme 3S: Synthetic route of **NaphMC-Ni(II)** complex.[3] [where S = solvent] (Yield: 67 mg, 81%).

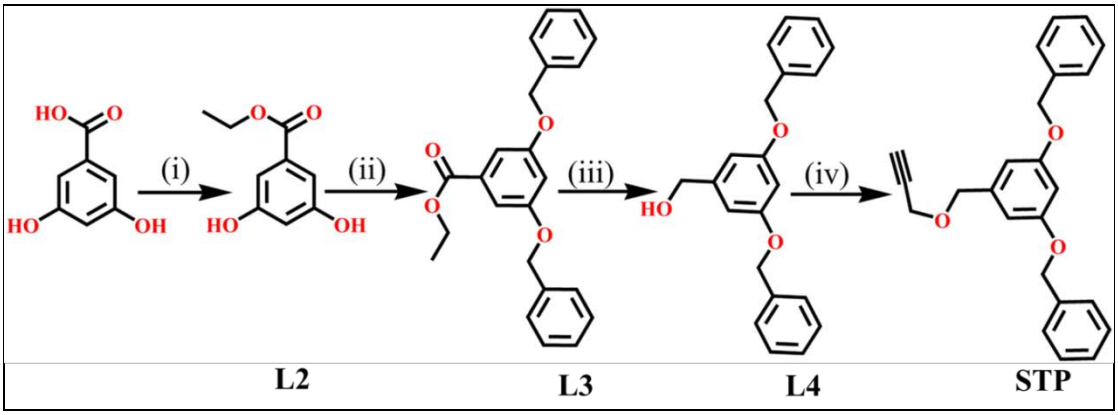

Scheme 4S: Synthetic route of stopper molecule (**STP**): (i) Ethanol, H_2SO_4, Reflux, 48 h, (yield: 692 mg, 95%); (ii) Benzyl bromide, K_2CO_3, CH_3CN, Reflux, 24 h, (yield: 913 mg, 84 %); (iii) $LiAlH_4$, Dry-THF, RT, 12 h, (yield: 208 mg, 65%); (iv) Propargyl bromide, NaH, 0^0C, 12 h, followed by refluxed for 12h, (yield: 272 mg, 76 %).

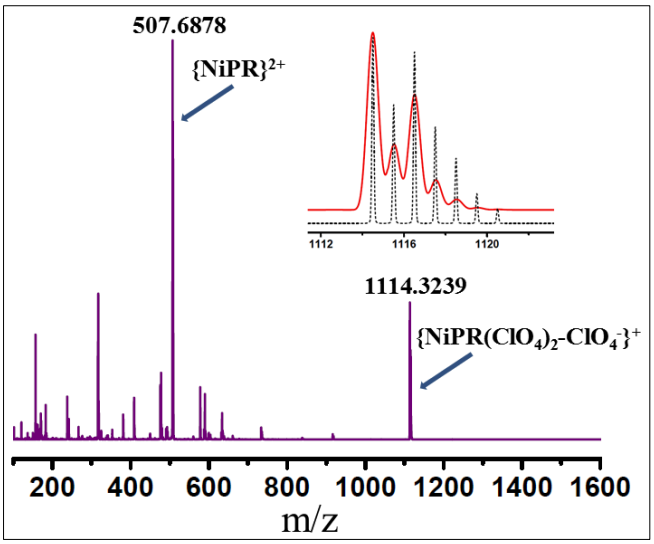

Figure 1S: ESI-MS (+ve) spectrum of [2]pseudorotaxane [**NiPR(ClO$_4$)$_2$**]. (Inset picture: isotopic distribution patterns).

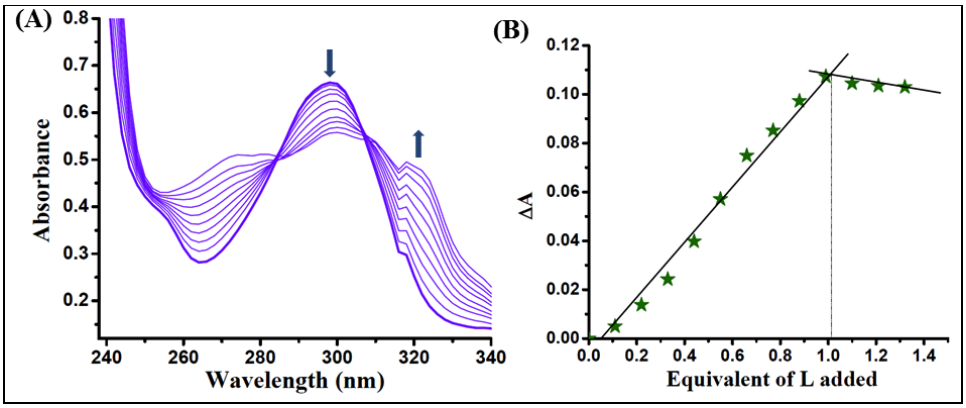

Figure 2S: UV/Vis titration profile of **L** ($2x10^{-5}$ M) with **NaphMC-Ni(II)** ($2.2x10^{-4}$ M) in CH_3CN and (B) Equivalence plot monitored at 298 nm for the formation of [**NiPR(ClO$_4$)$_2$**].

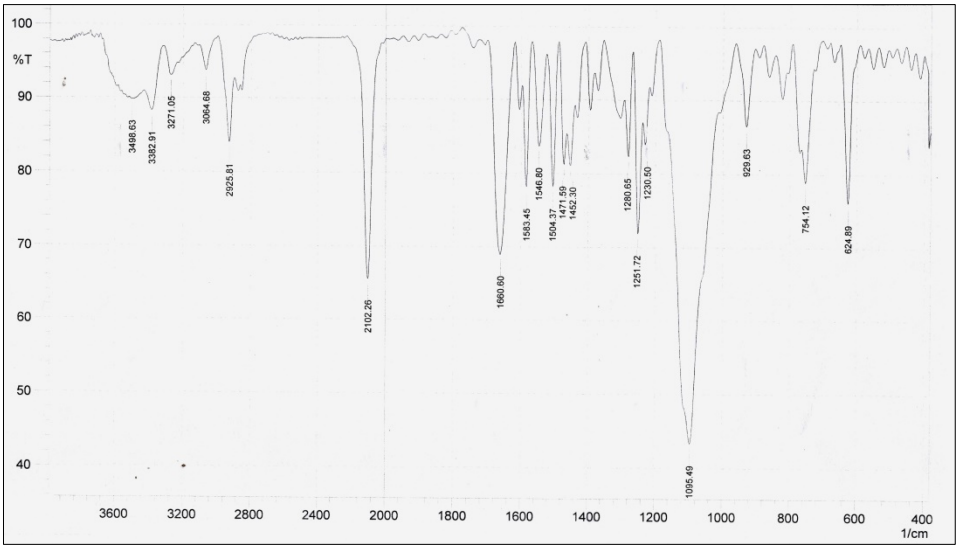

Figure 3S: IR spectrum of [**NiPR(ClO$_4$)$_2$**].

Characterization of **L3:**

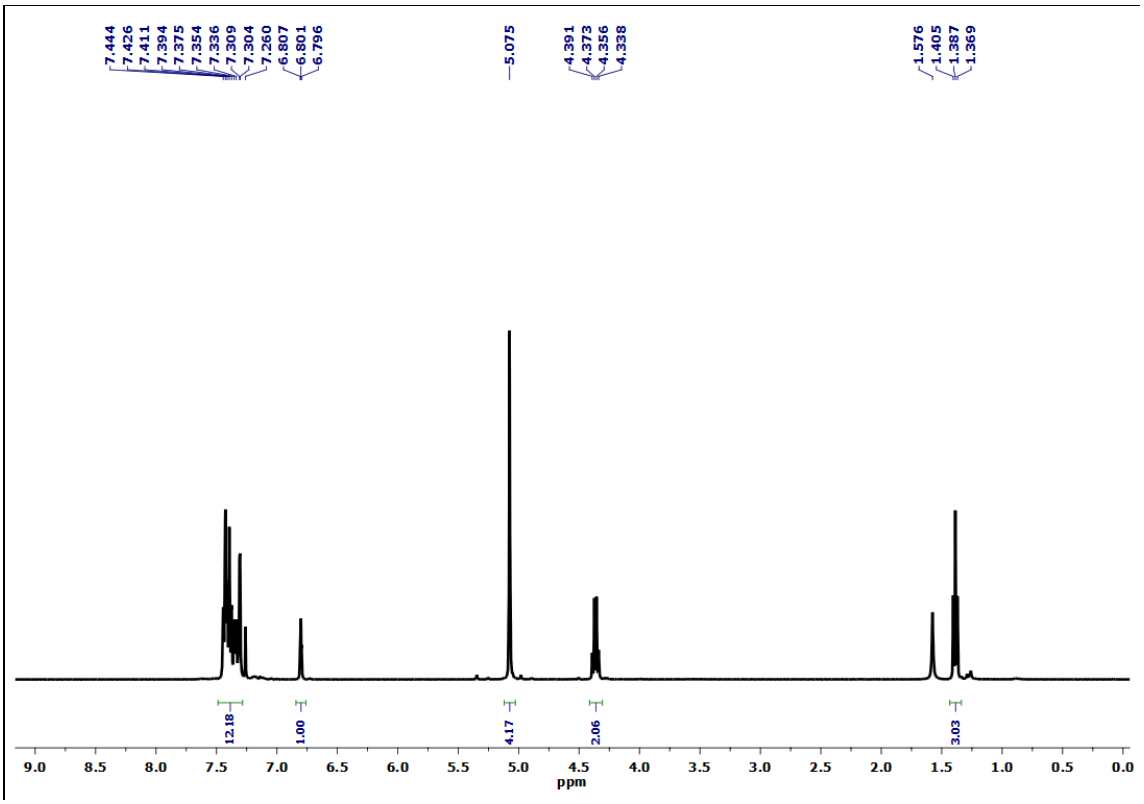

Figure 4S: ^{1}H-NMR spectrum of **L3** in $CDCl_3$ in 400 MHz at 298K.

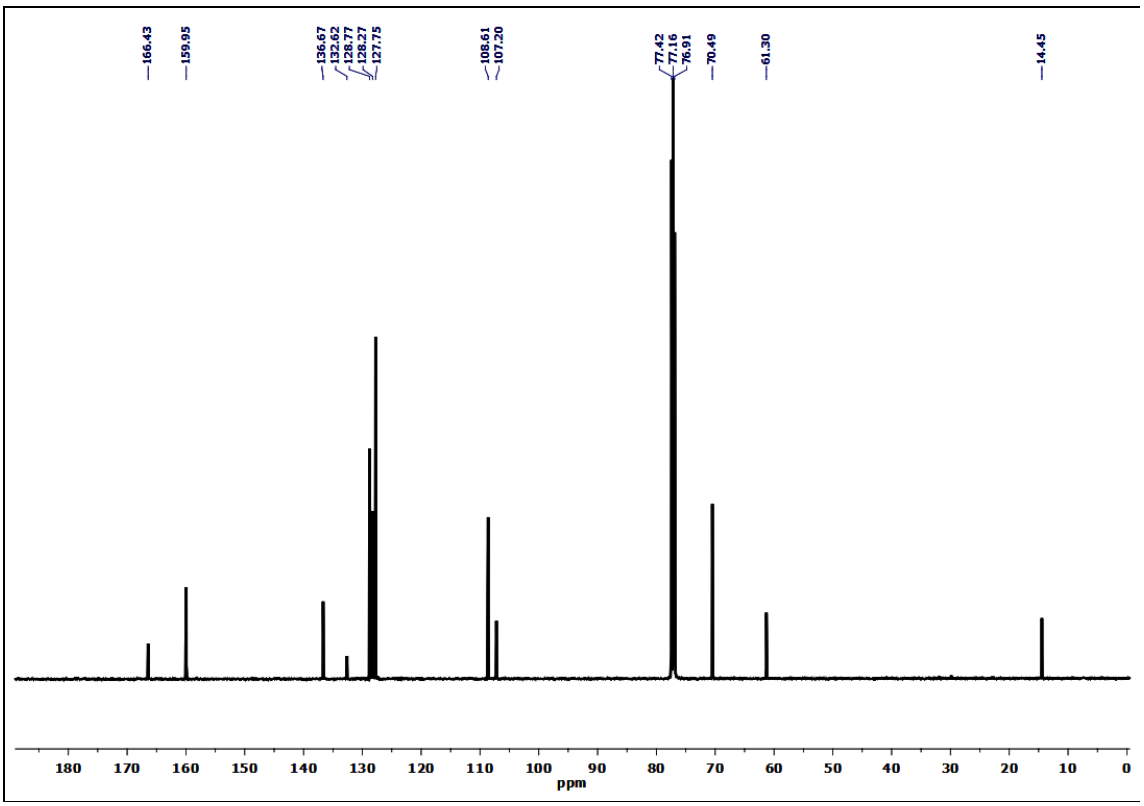

Figure 5S: ^{13}C-NMR spectrum of **L3** in $CDCl_3$ in 125 MHz at 298K.

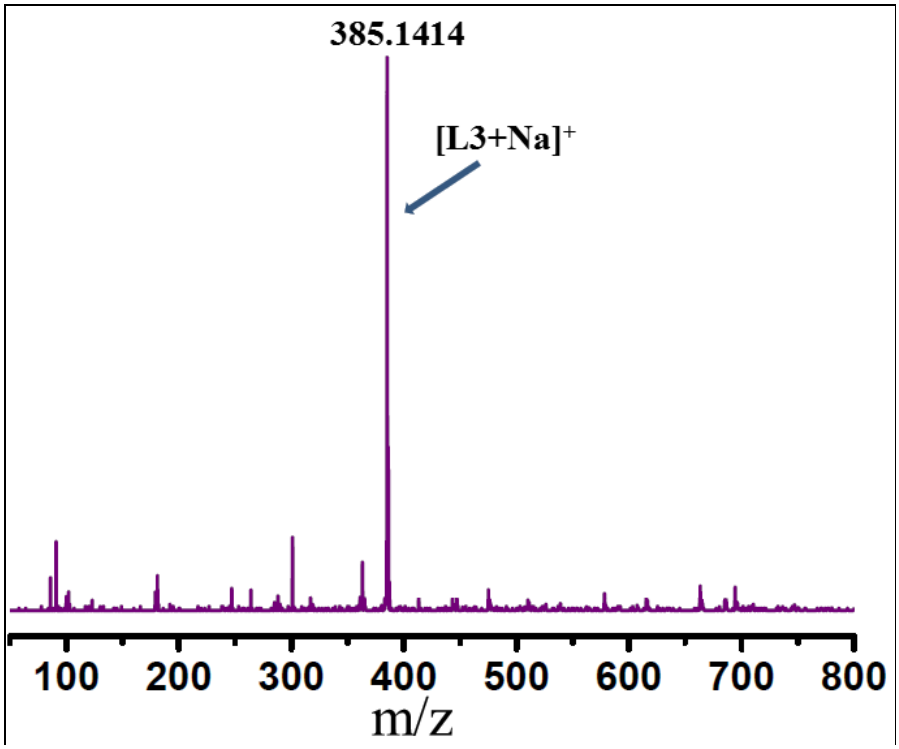

Figure 6S: ESI-MS (+ve) spectrum of **L3.**

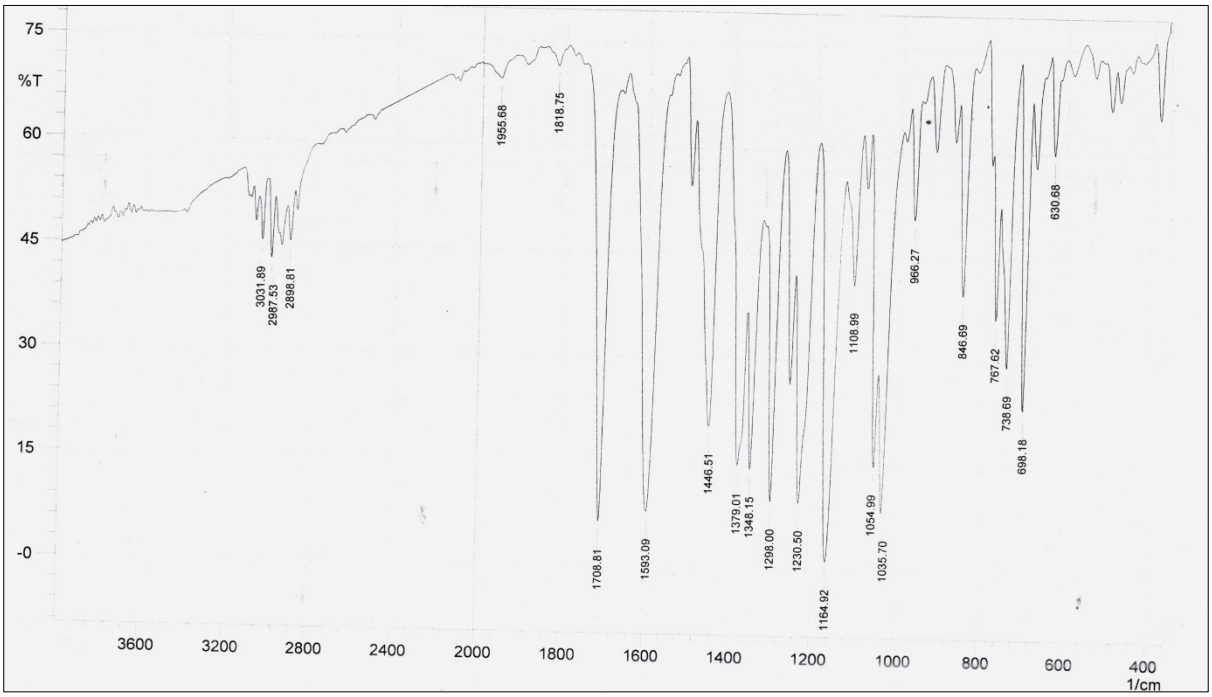

Figure 7S: IR spectrum of **L3.**

Characterization of **L4:**

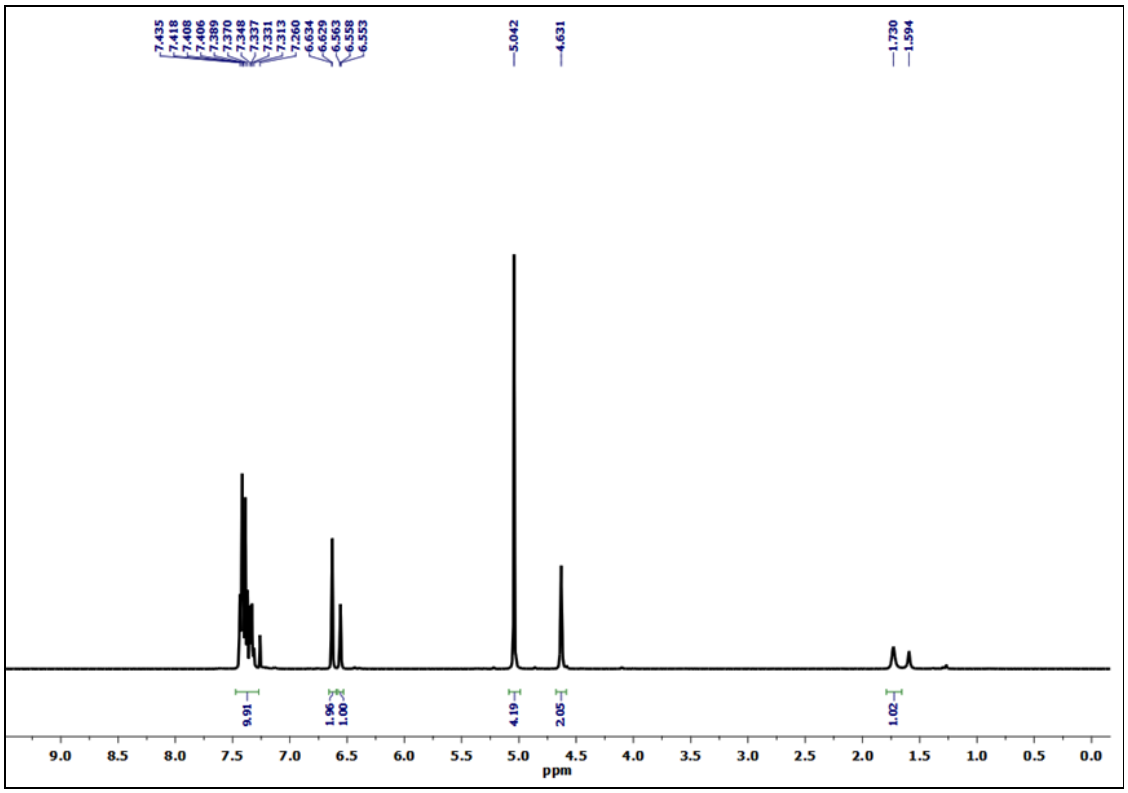

Figure 8S: ^{1}H-NMR spectrum of **L4** in $CDCl_3$ in 400 MHz at 298K.

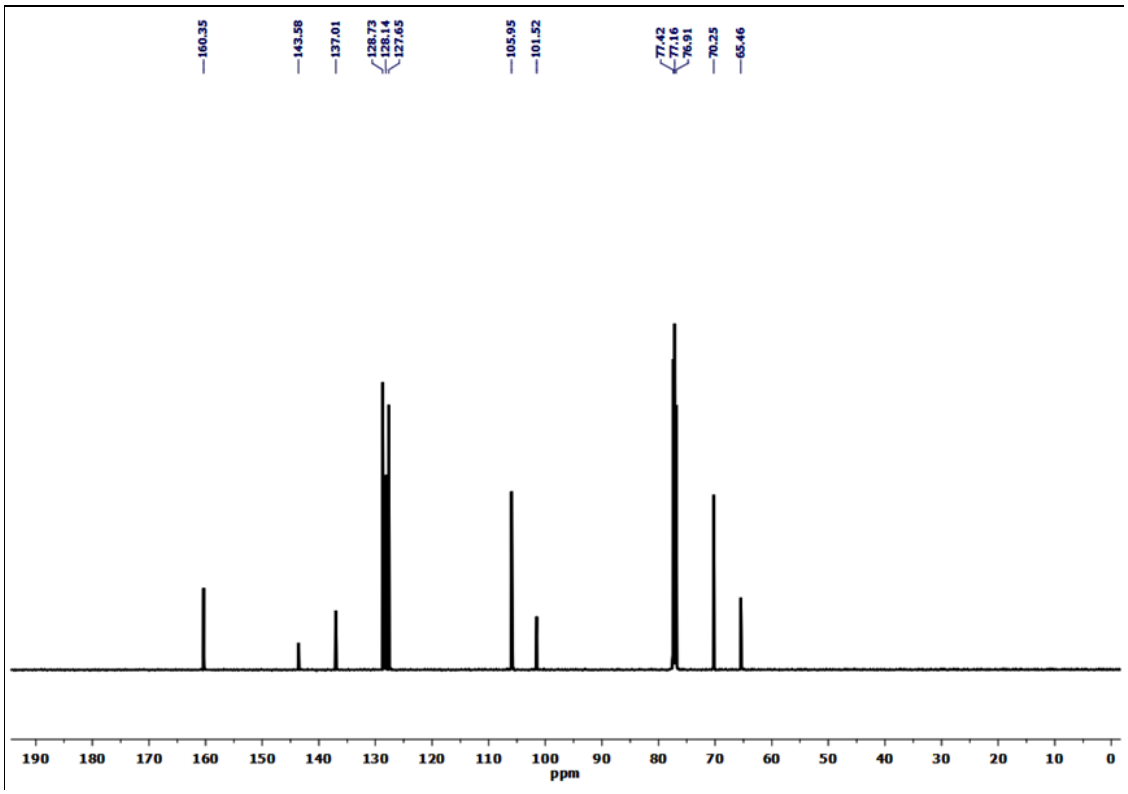

Figure 9S: ^{13}C-NMR spectrum of **L4** in $CDCl_3$ in 125 MHz at 298K.

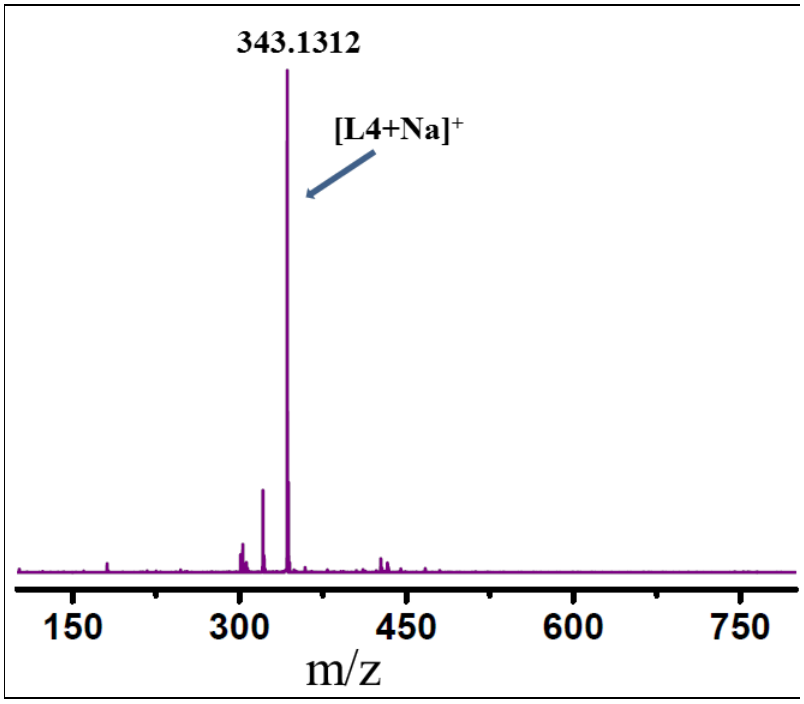

Figure 10S: ESI-MS(+ve) spectrum of **L4.**

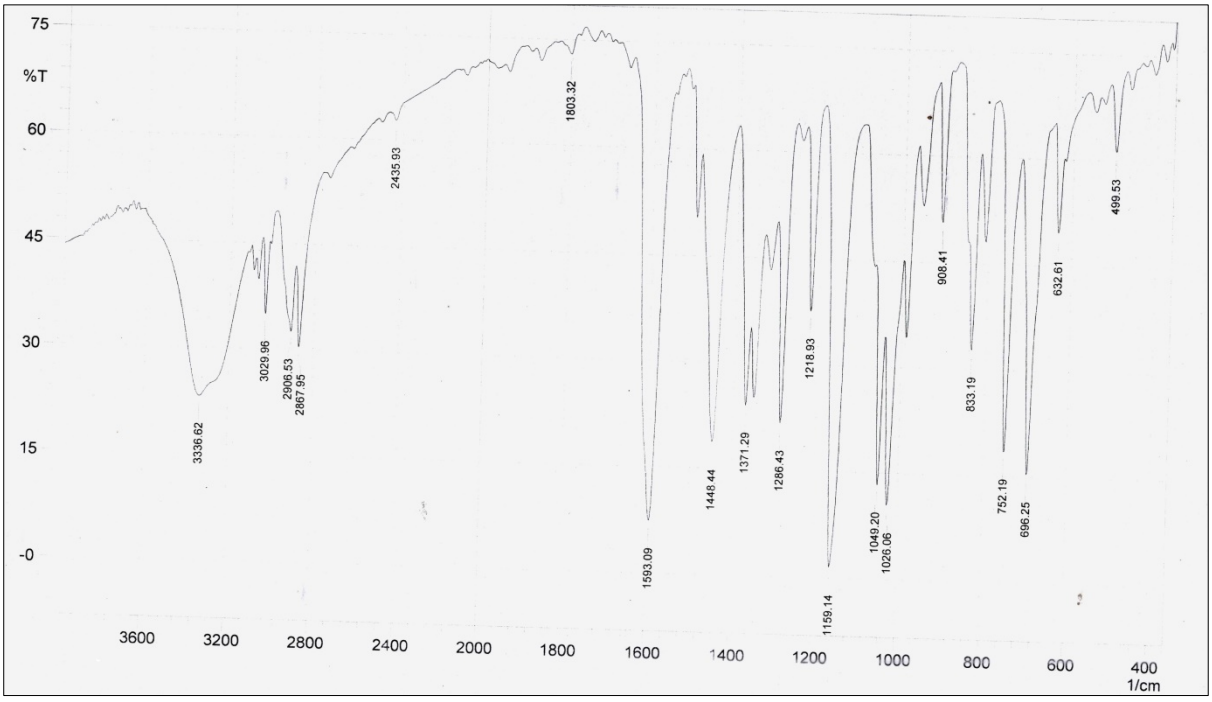

Figure 11S: IR spectrum of **L4.**

Characterization of **STP:**

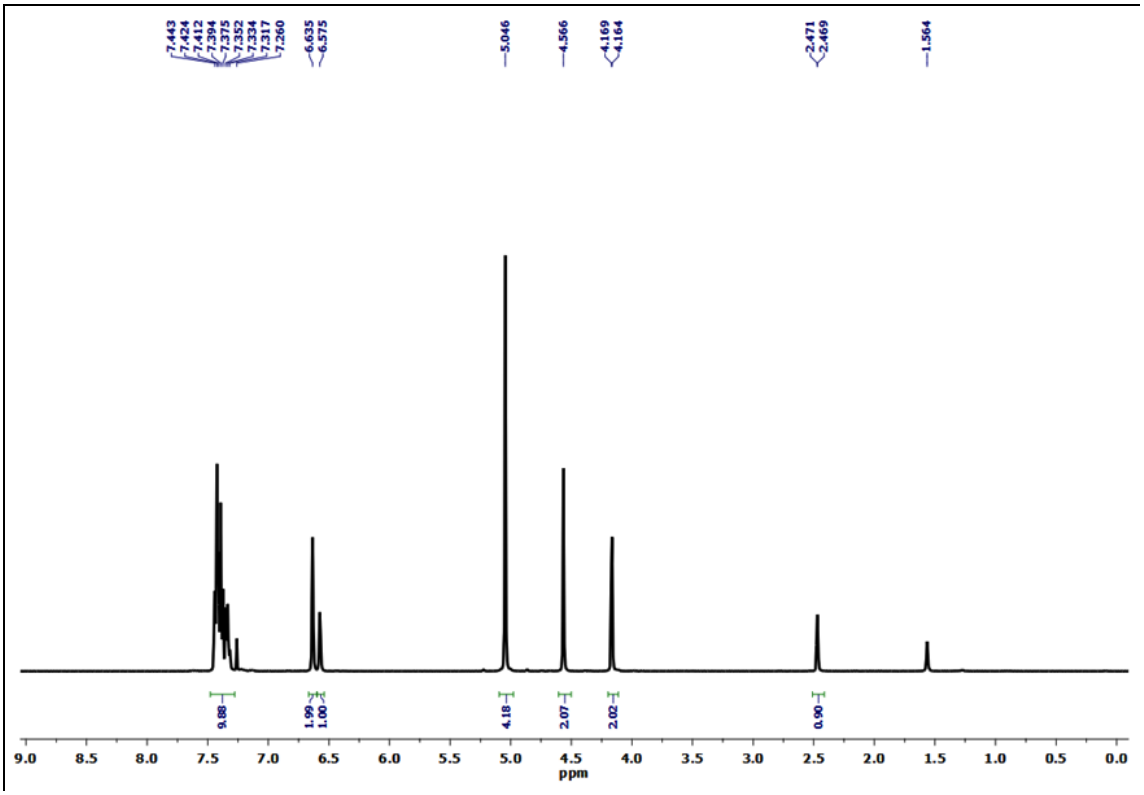

Figure 12S: ^{1}H-NMR spectrum of **STP** in $CDCl_3$ in 400 MHz at 298K.

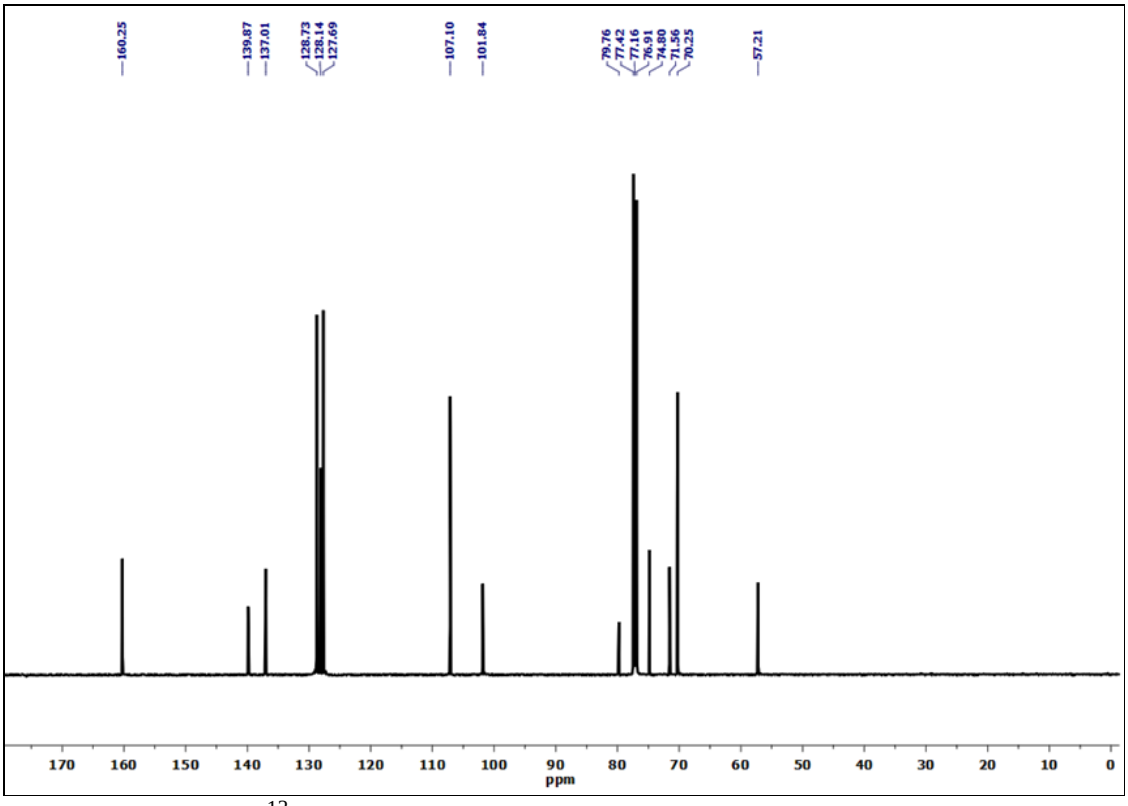

Figure 13S: ^{13}C-NMR spectrum of **STP** in $CDCl_3$ in 125 MHz at 298K.

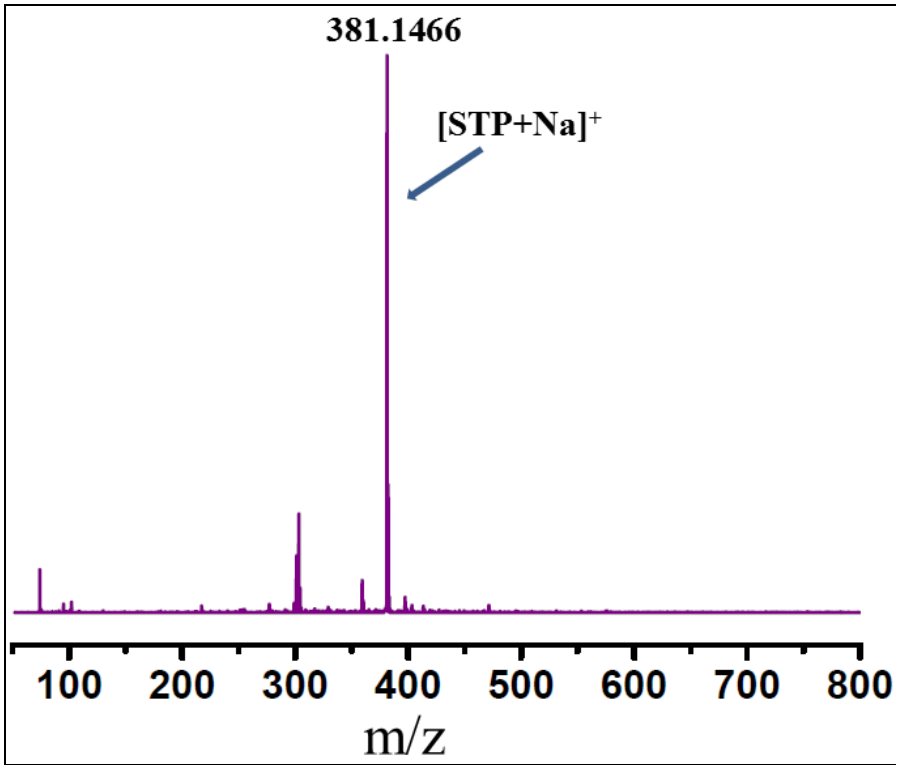

Figure 14S: ESI-MS (+ve) spectrum of **STP.**

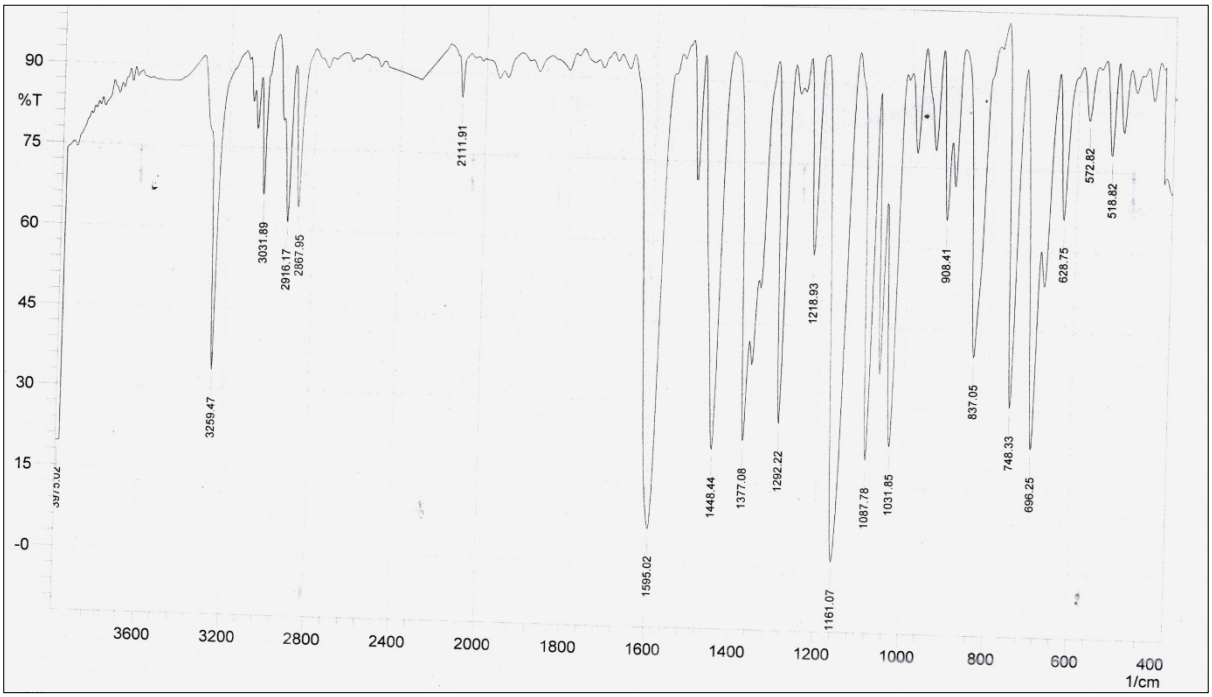

Figure 15S: IR spectrum of **STP.**

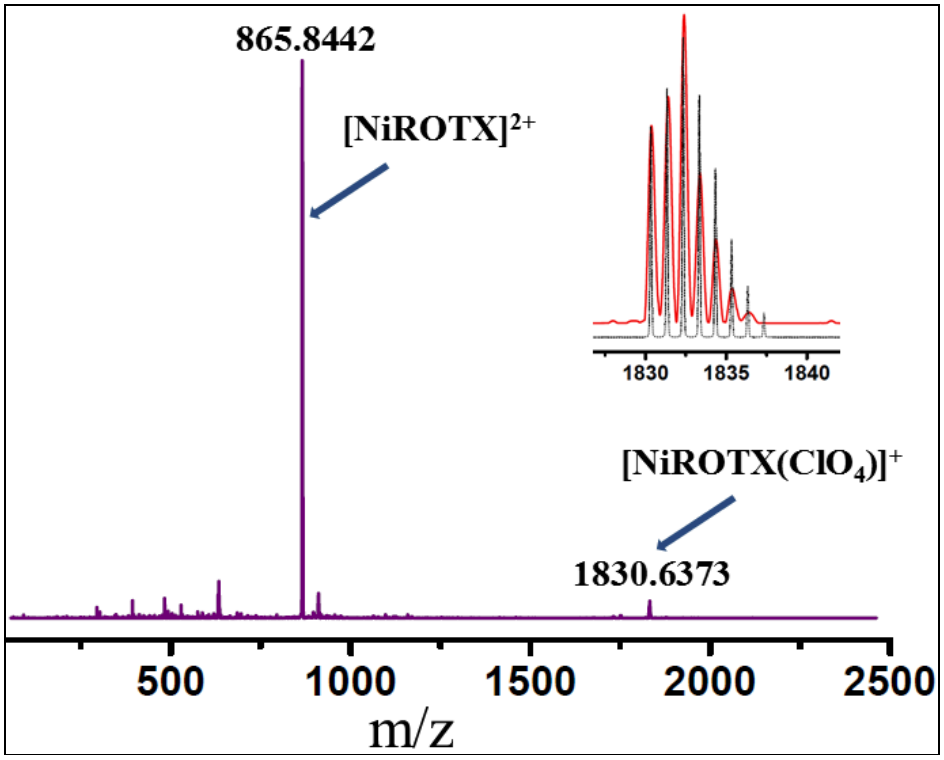

Figure 16S: ESI-MS (+ve) spectrum of **metallated [2]rotaxane {NiROTX(ClO_4)$_2$}.**

Characterization of **ROTX:**

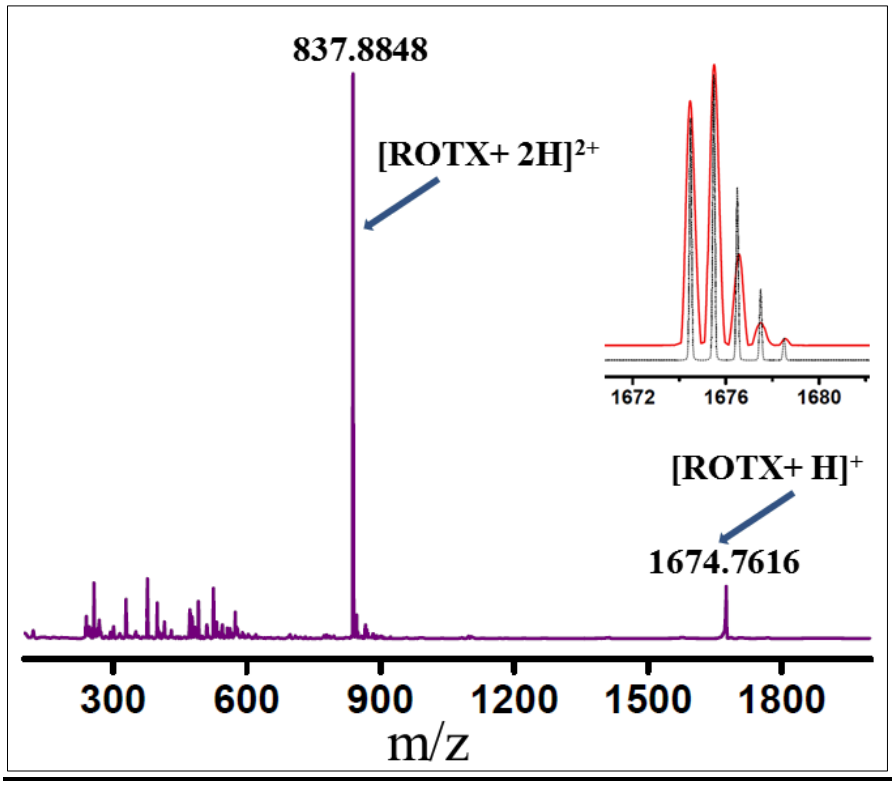

Figure 17S: ESI-MS (+ve) spectrum of [2]rotaxane {**ROTX**}. (Inset picture shows the red line for experimental and black line for calculated isotopic distribution patterns respectively).

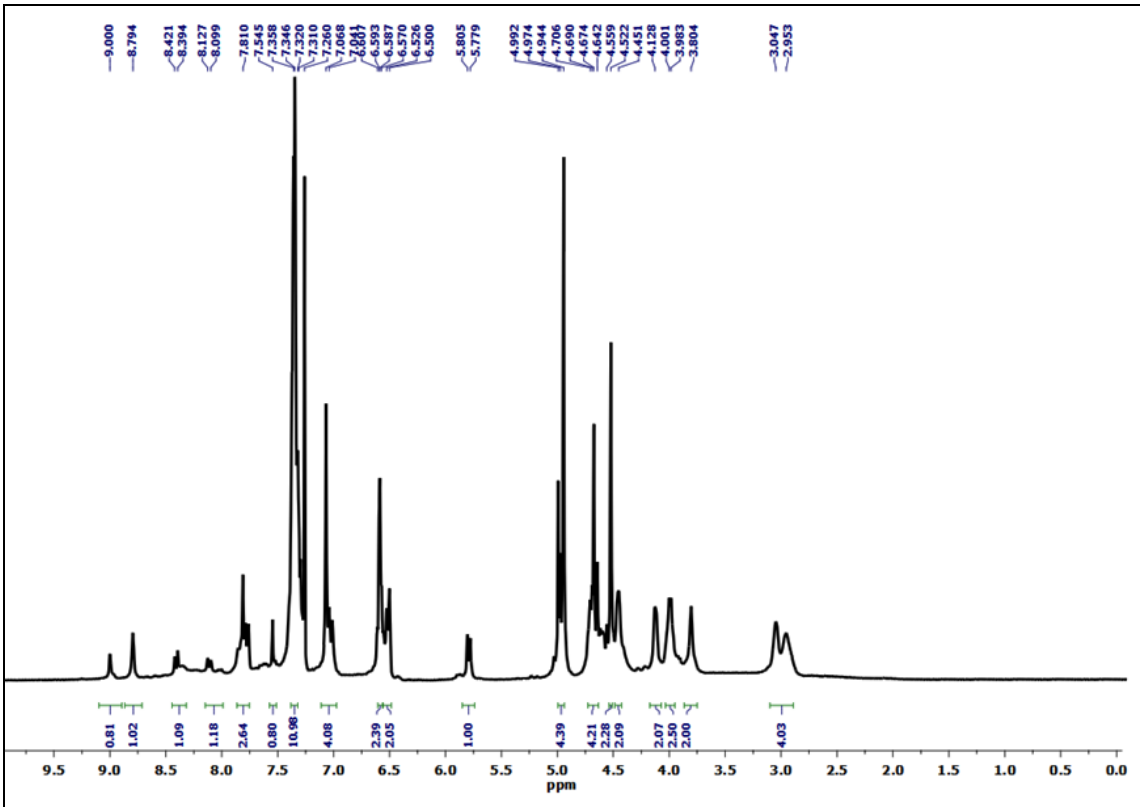

Figure 18S: ^{1}H-NMR spectrum of rotaxane (**ROTX**) in $CDCl_3$ in 300 MHz at 298K.

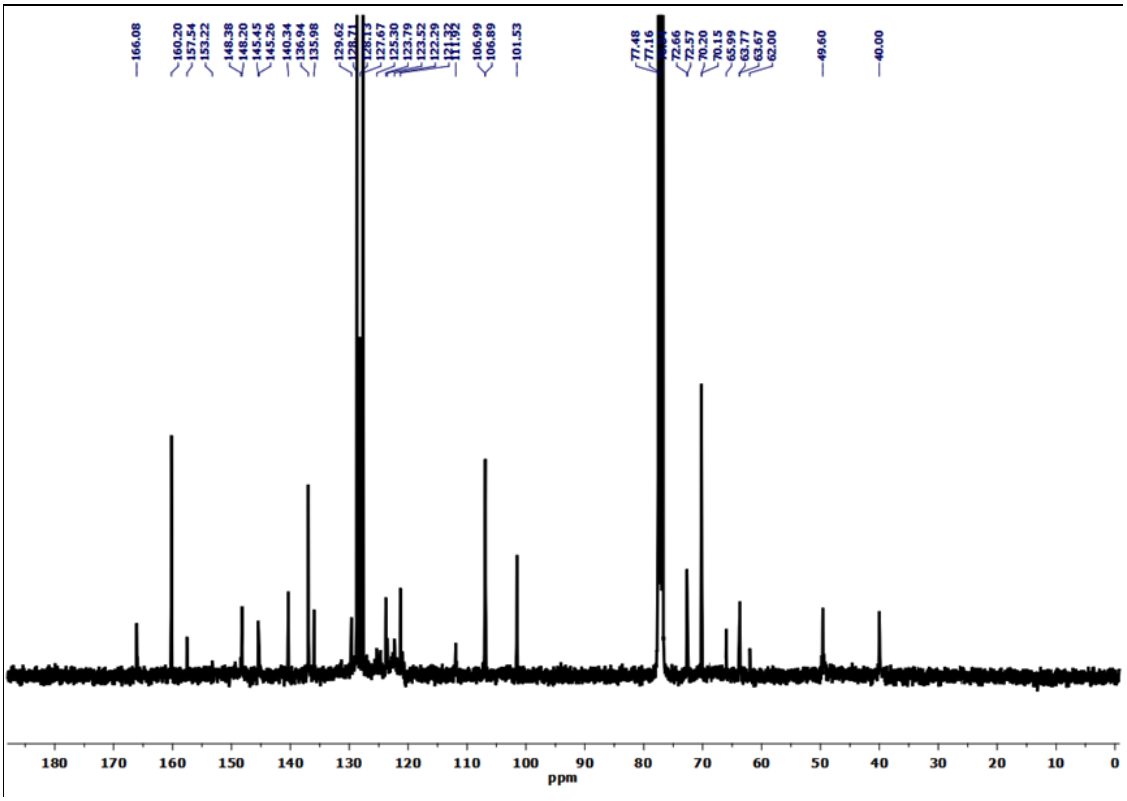

Figure 19S: ^{13}C-NMR spectrum of rotaxane (**ROTX**) in $CDCl_3$ in 100 MHz at 298K.

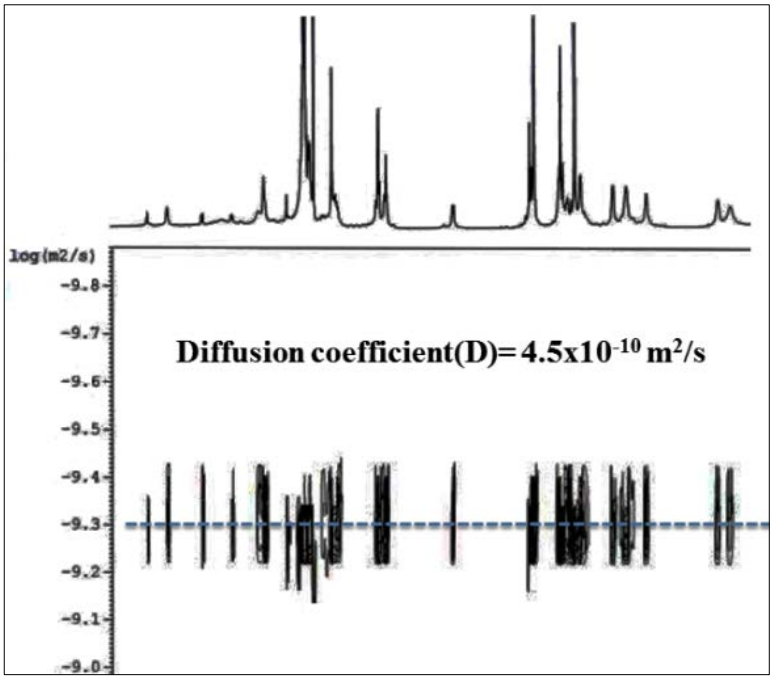

Figure 20S: DOSY spectrum in $CDCl_3$ of [2]rotaxane (**ROTX**).

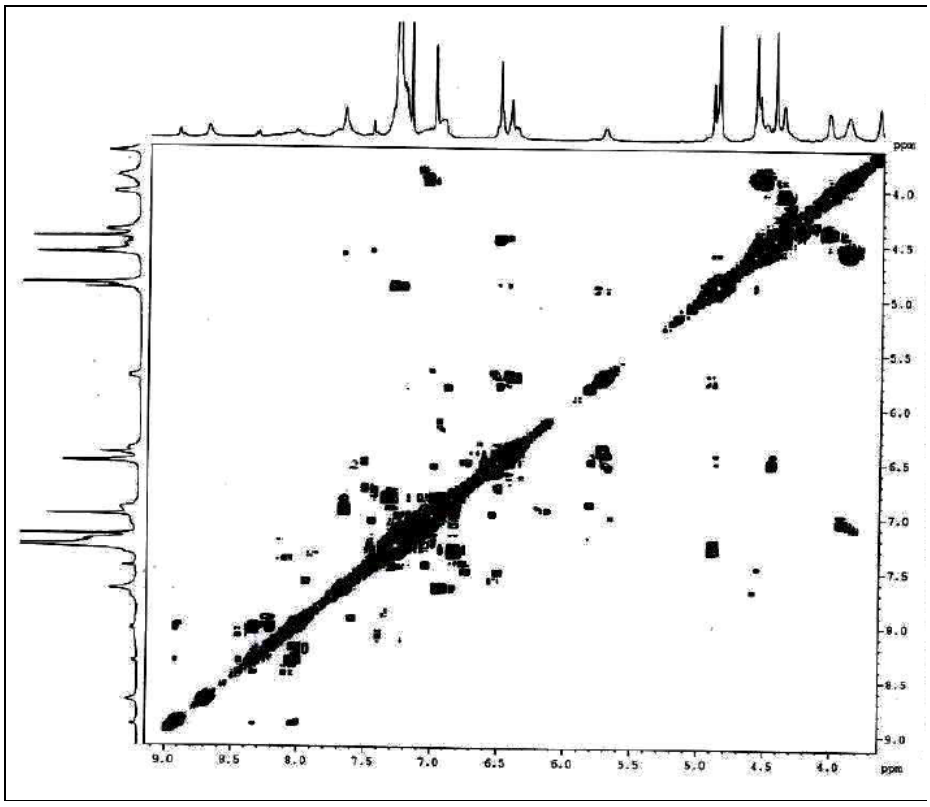

Figure 21S: COSY-NMR spectrum of **ROTX** in $CDCl_3$ in 400 MHz at 298K.

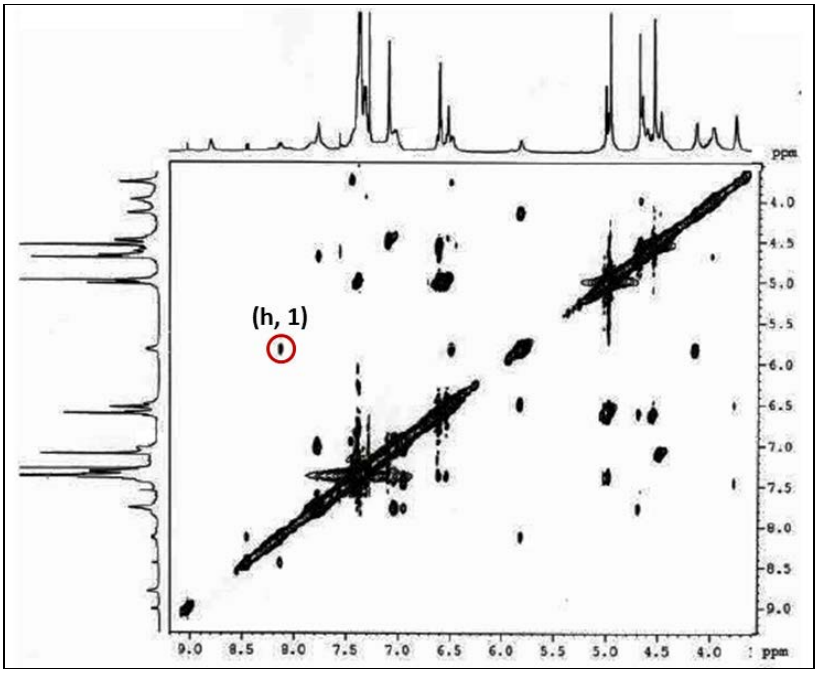

Figure 22S. ROESY-NMR spectrum of **ROTX** in $CDCl_3$ in 400 MHz at 298K.

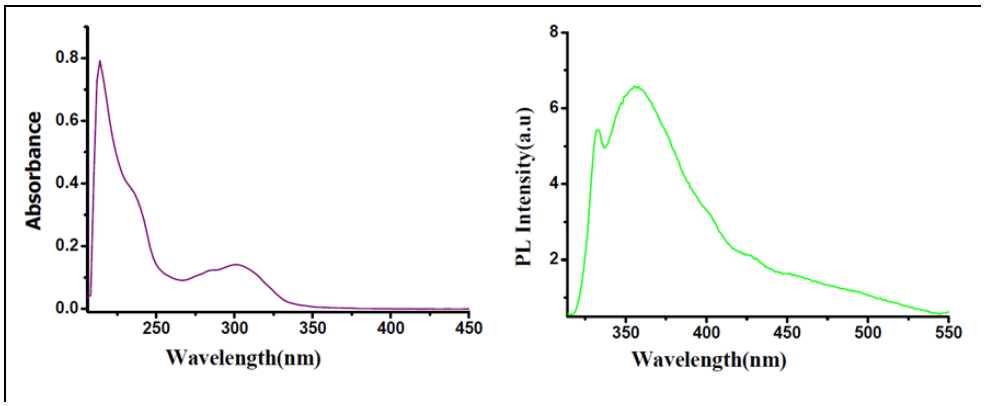

Figure 23S: Characteristic (A) absorption and (B) emission spectra of **ROTX** in dry THF at 298 K, λ_{exc}= 302 nm.

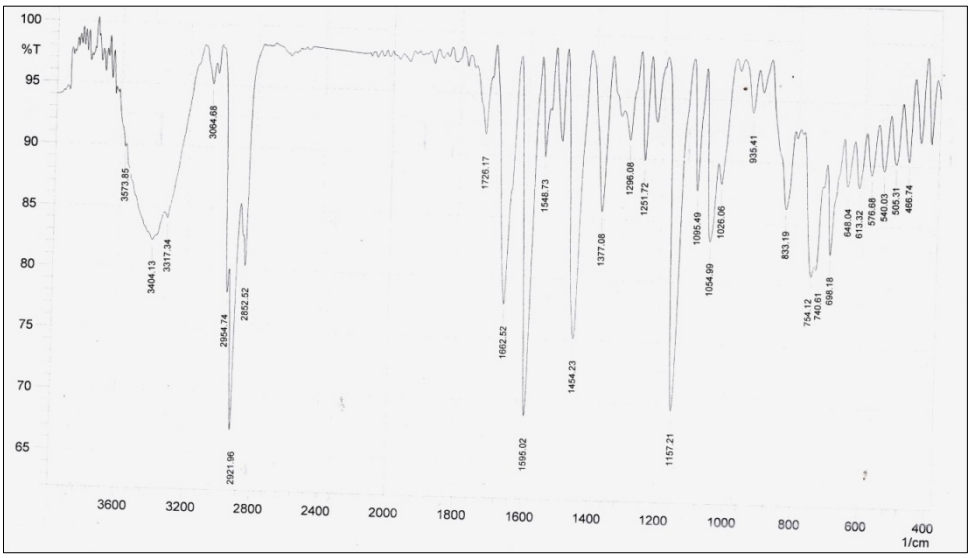

Figure 24S: IR spectrum of **ROTX**.

Characterization of **AXLE:**

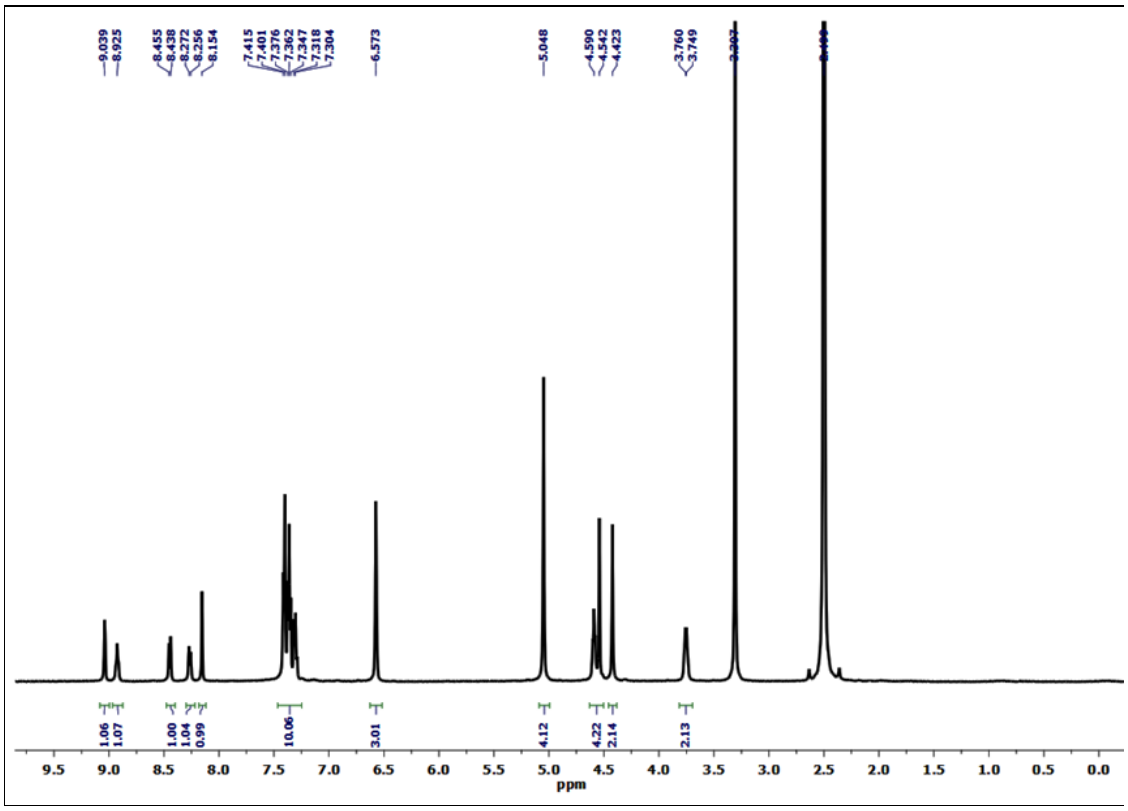

Figure 25S: ^{1}H-NMR spectrum of **AXLE** in DMSO-d_6 in 500 MHz at 298K.

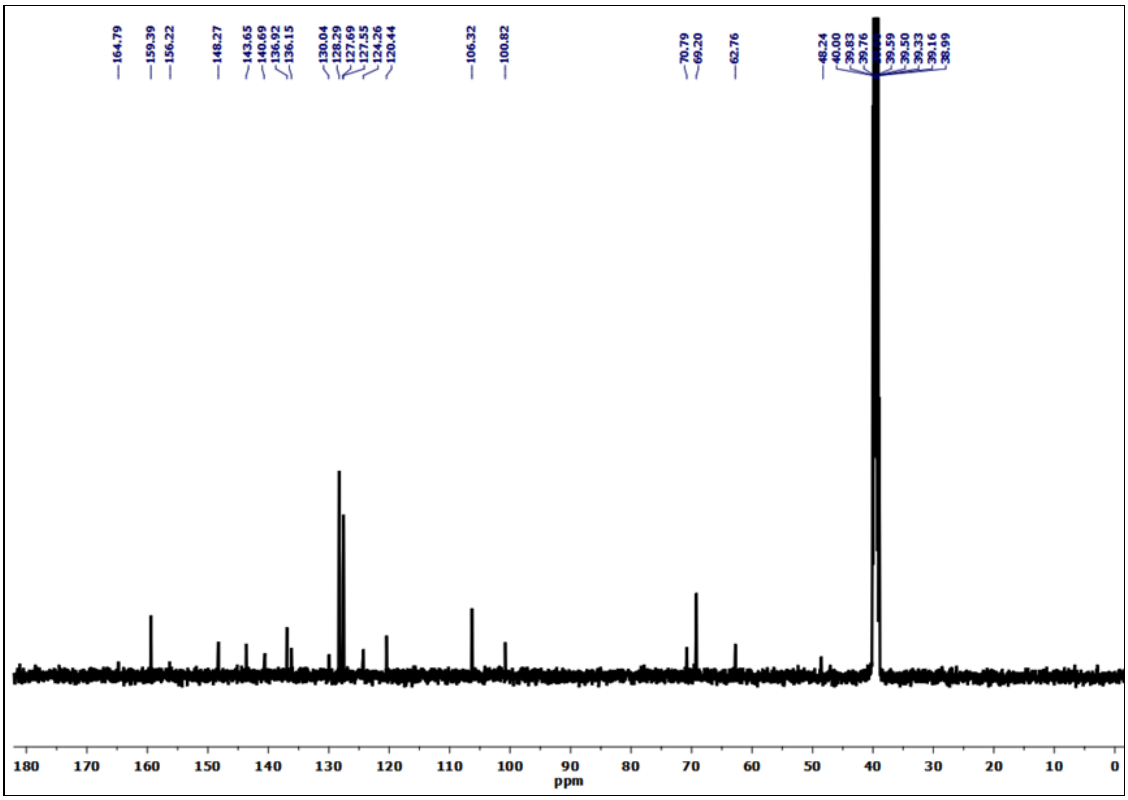

Figure 26S: ^{13}C-NMR spectrum of **AXLE** in DMSO-d_6 in 125 MHz at 298K.

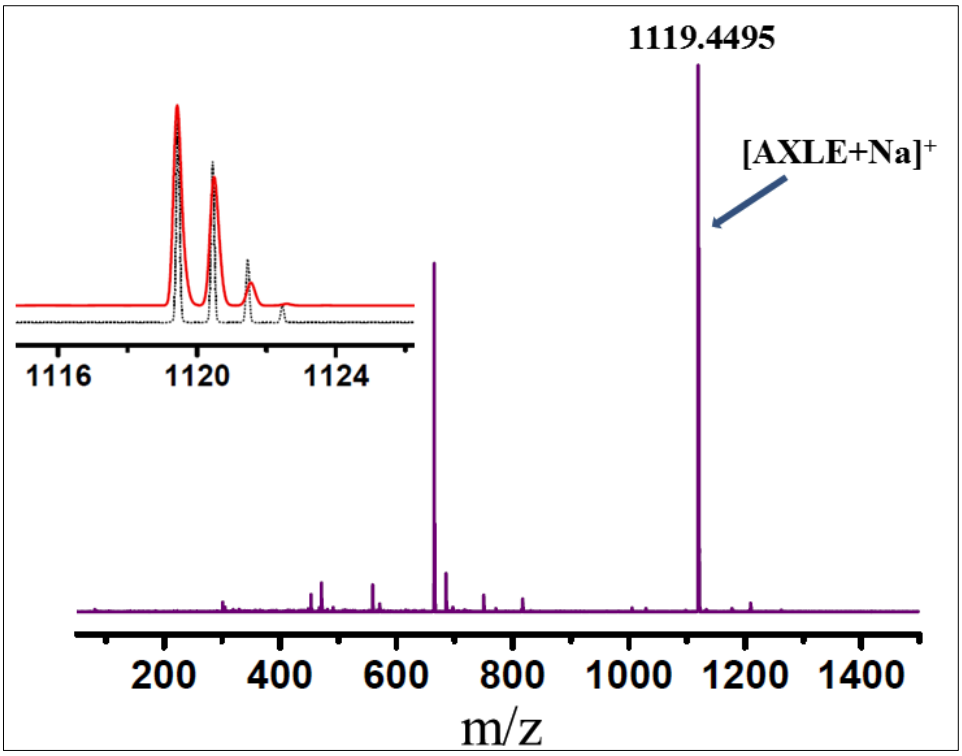

Figure 27S: ESI-MS (+ve) spectrum of **AXLE.**

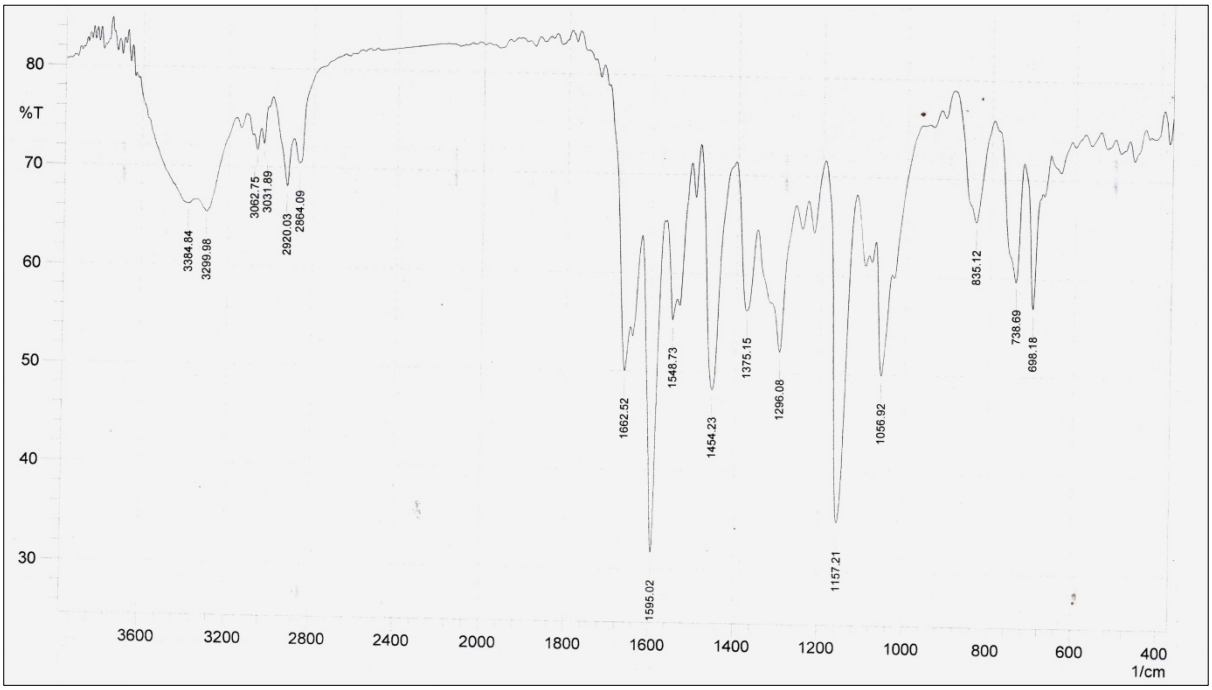

Figure 28S: IR spectrum of **AXLE.**

Characterization of **PYROTX:**

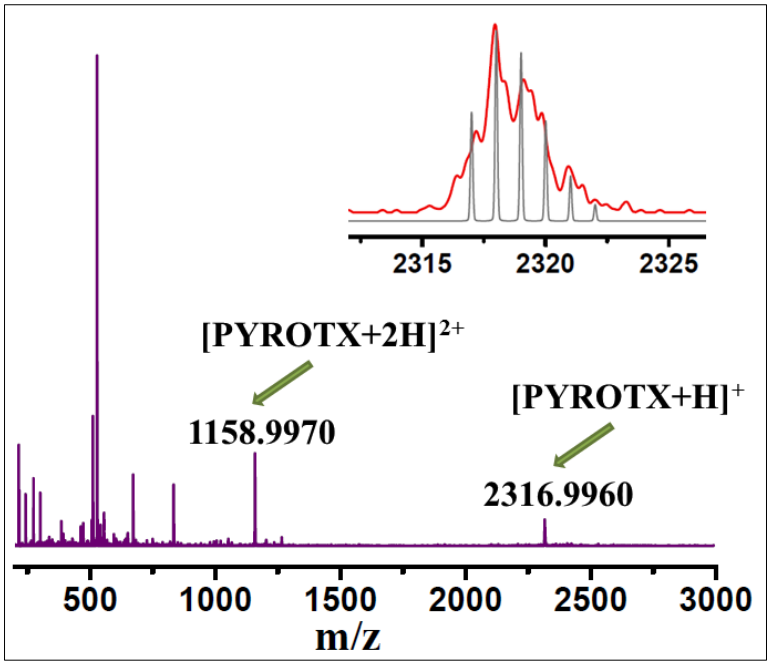

Figure 29S: ESI-MS (+ve) spectrum of **PYROTX**. (Inset picture shows the red line for experimental and black line for calculated isotopic distribution patterns respectively).

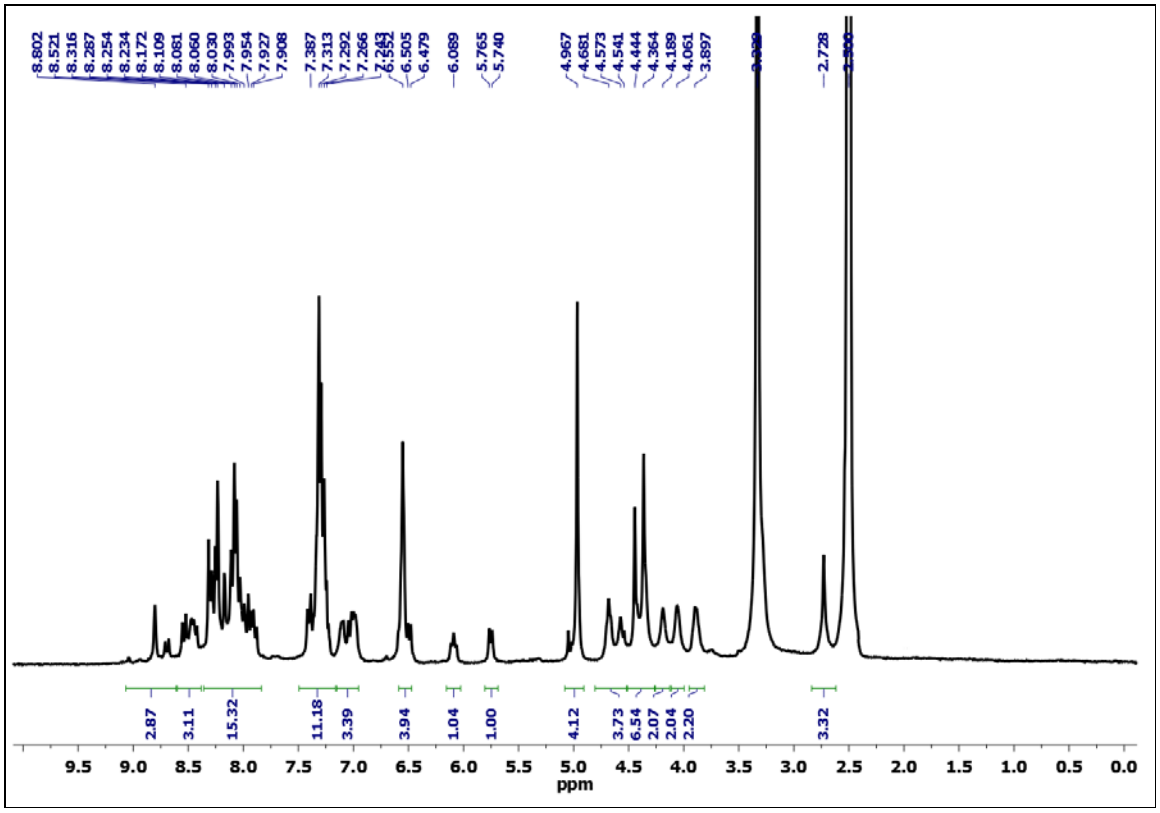

Figure 30S: ^{1}H-NMR spectrum of **PYROTX** in DMSO-d_6 in 300 MHz at 300K.

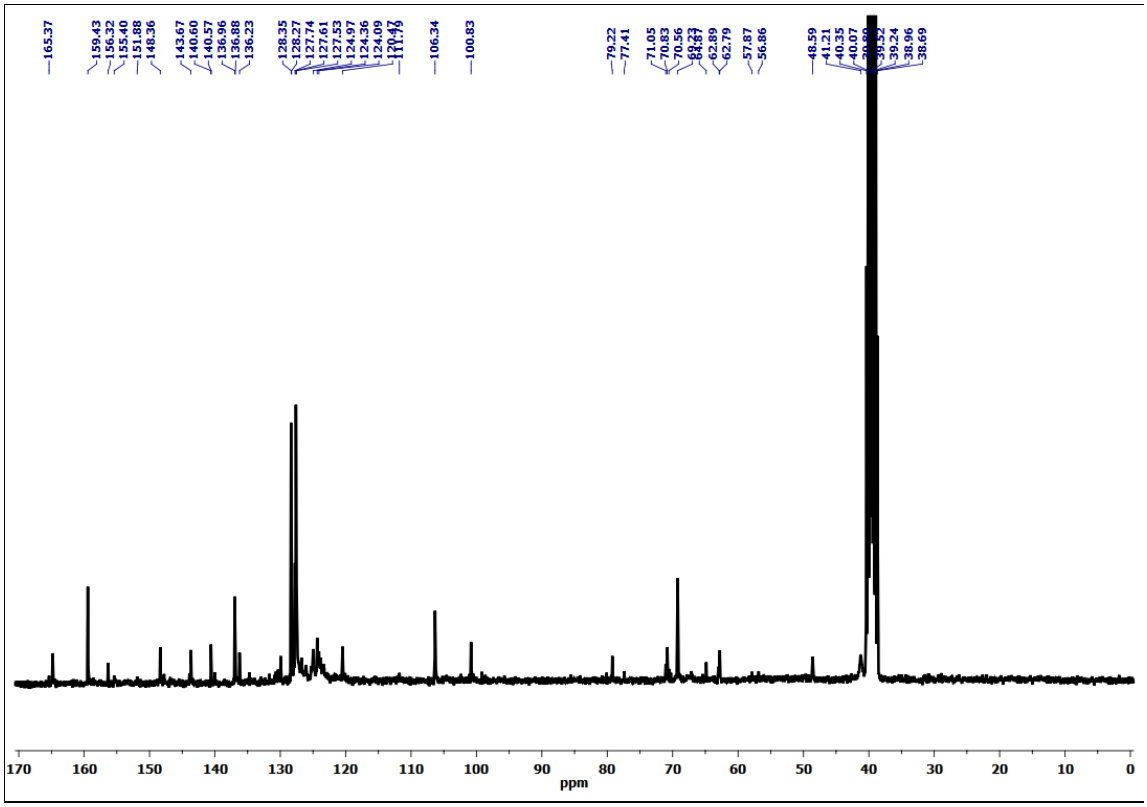

Figure 31S: ^{13}C-NMR spectrum of **PYROTX** in DMSO-d_6 in 75 MHz at 300K.

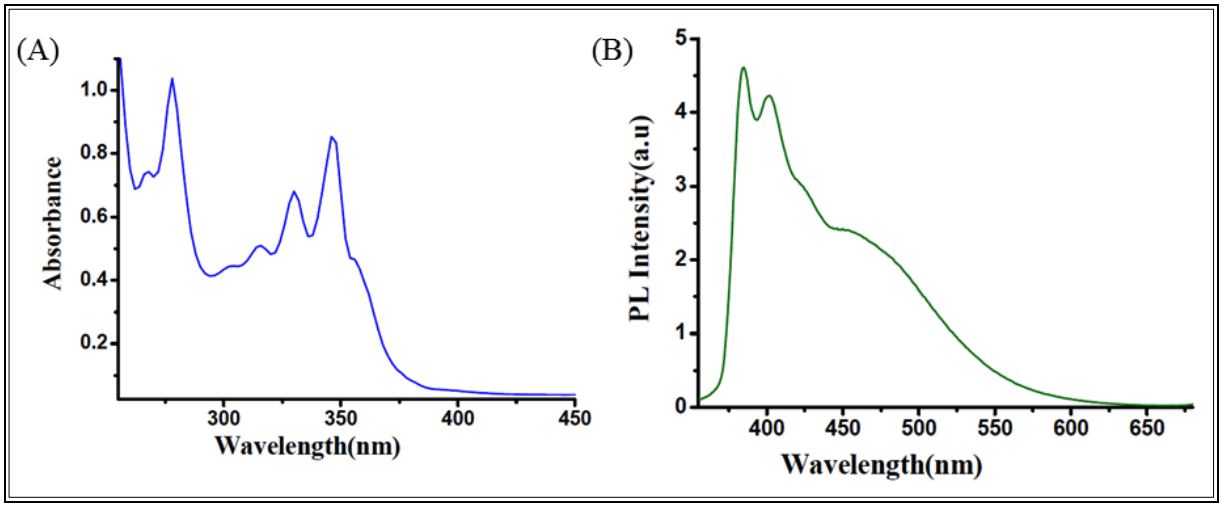

Figure 32S: Characteristic (A) absorption and (B) emission spectra of **PYROTX** in dry THF at 298 K, λ_{exc}= 346 nm.

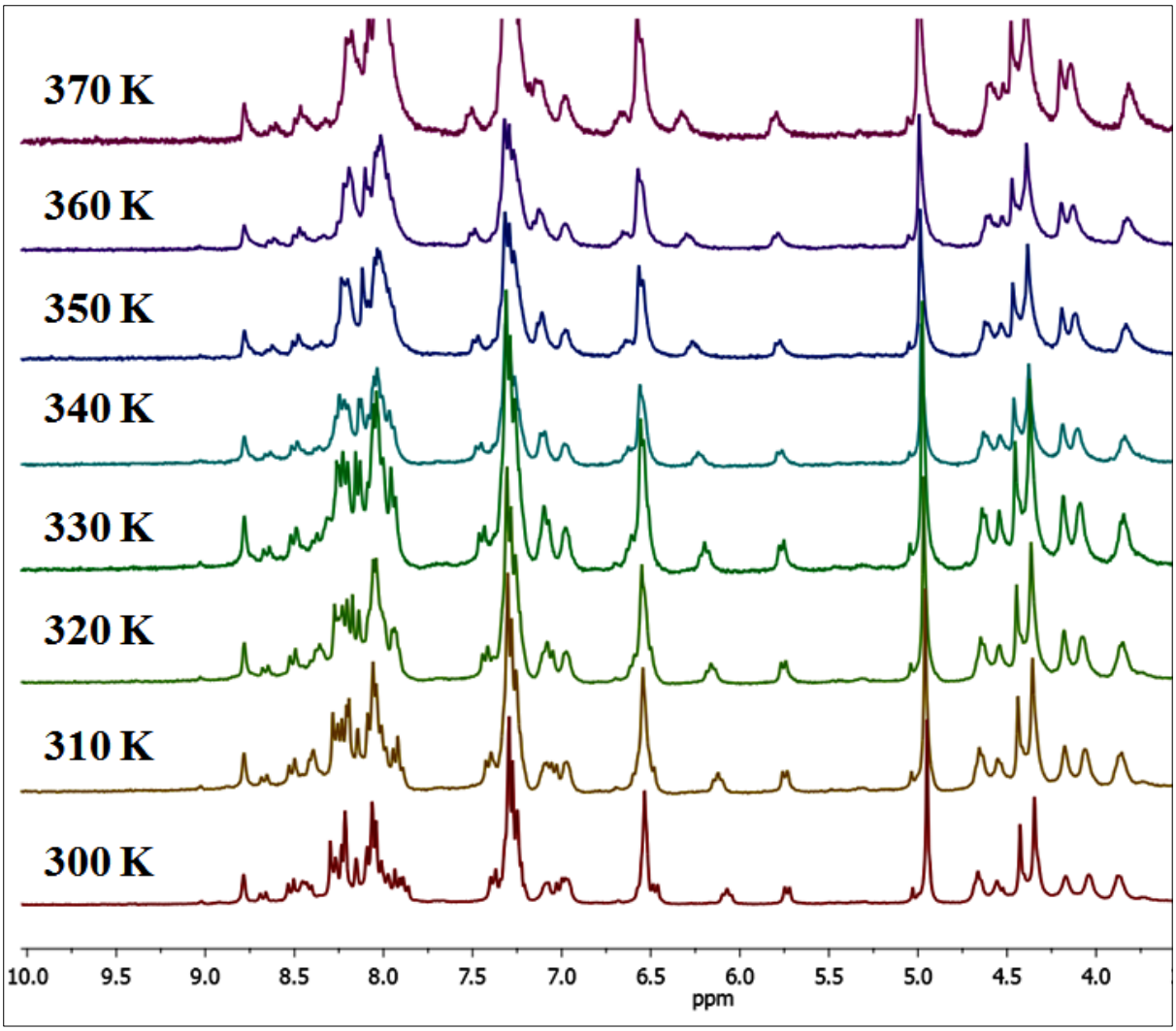

Figure 33S. Variable temperatures ^{1}H NMR stacked plot of **PYROTX** in DMSO-d_6 (300 MHz).

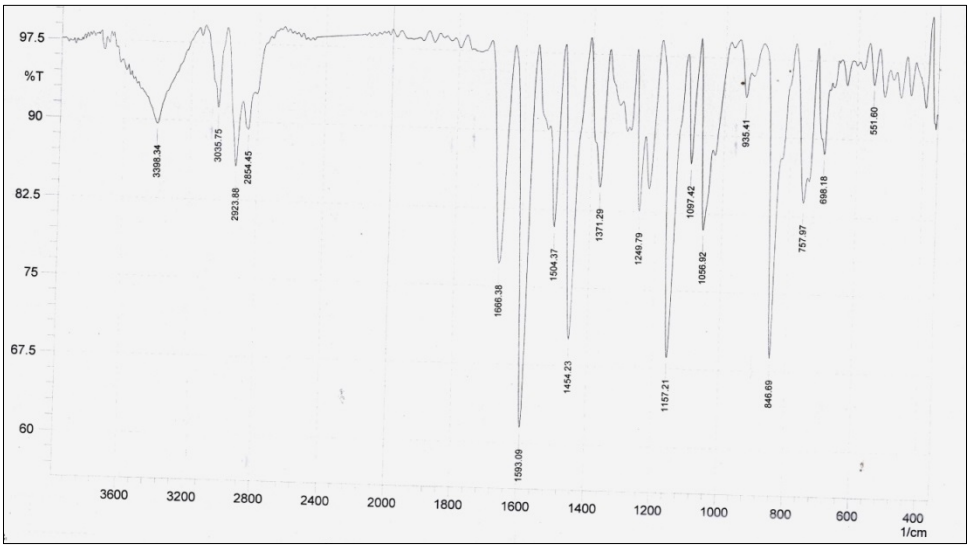

Figure 34S: Characteristic IR spectrum of **PYROTX**.

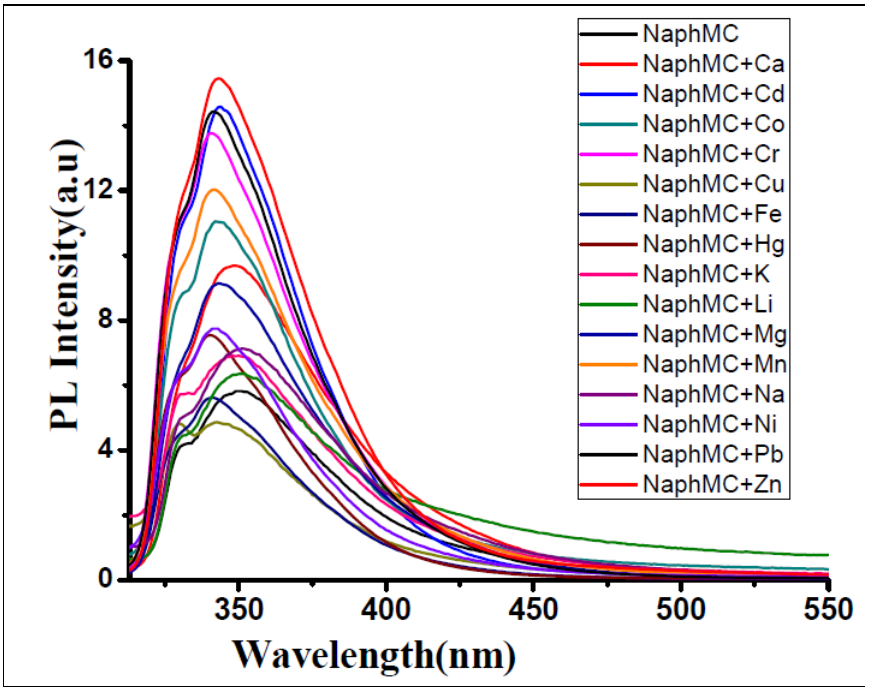

Figure 35S: Emission spectra of **NaphMC** ($5x10^{-6}$ M) in the presence of 10 equivalents of Ni^{2+}, Cu^{2+}, Mn^{2+}, Cr^{3+}, Co^{2+}, Hg^{2+}, Cd^{2+}, Li^{+}, Na^{+}, K^{+}, Ca^{2+}, Fe^{3+}, Mg^{2+}, Zn^{2+} and Pb^{2+} ion in THF at 298 K, λ_{exc}= 300 nm.

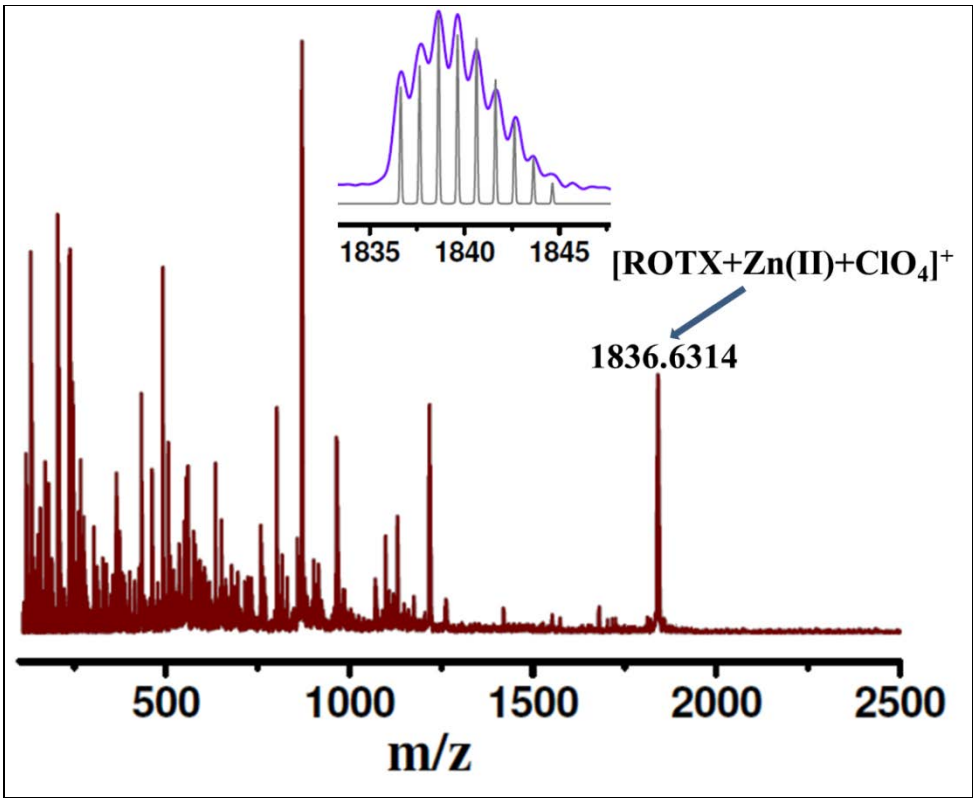

Figure 36S: ESI-MS spectrum of pale yellow coloured **Zn^{2+}**-bound **ROTX**.

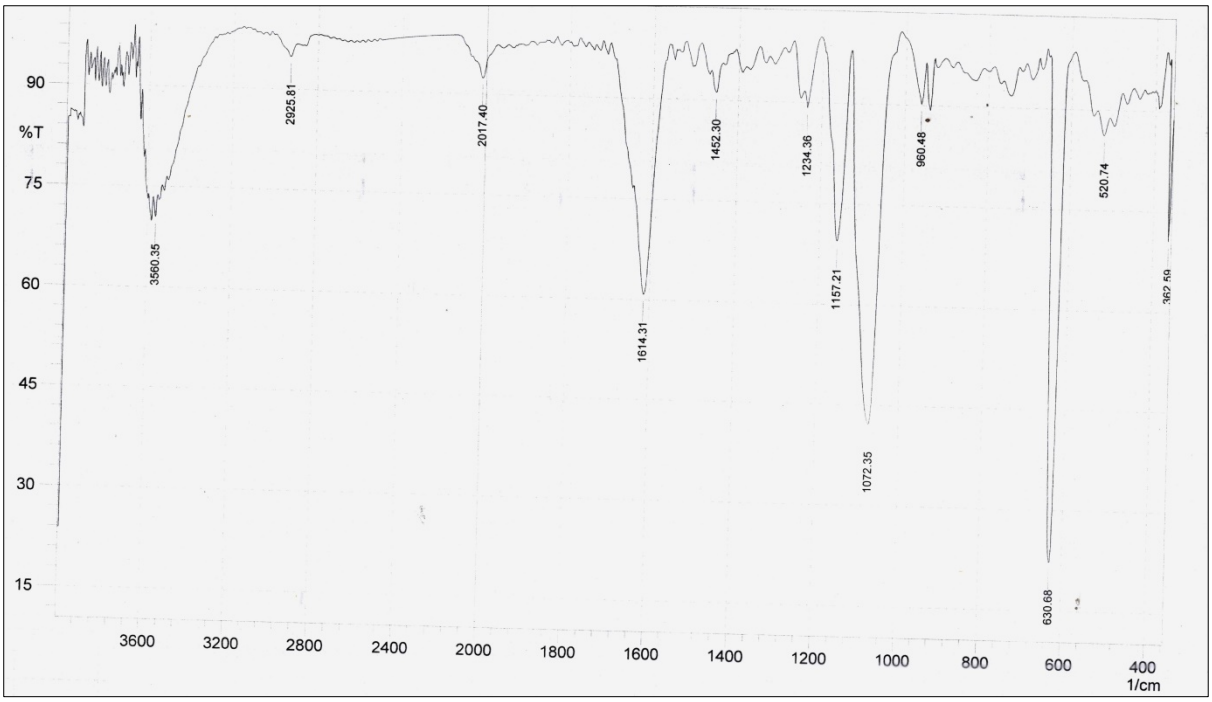

Figure 37S: IR spectrum of **Zn^{2+}**-bound **ROTX**.

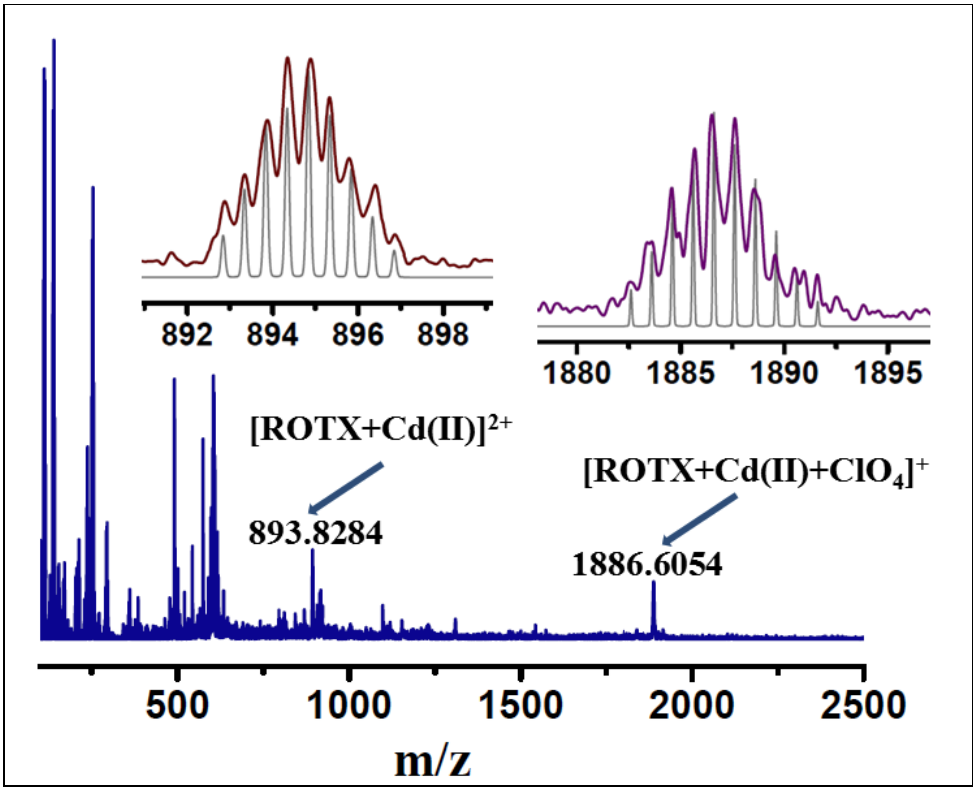

Figure 38S: ESI-MS spectrum of yellow coloured **Cd^{2+}**-bound **ROTX**.

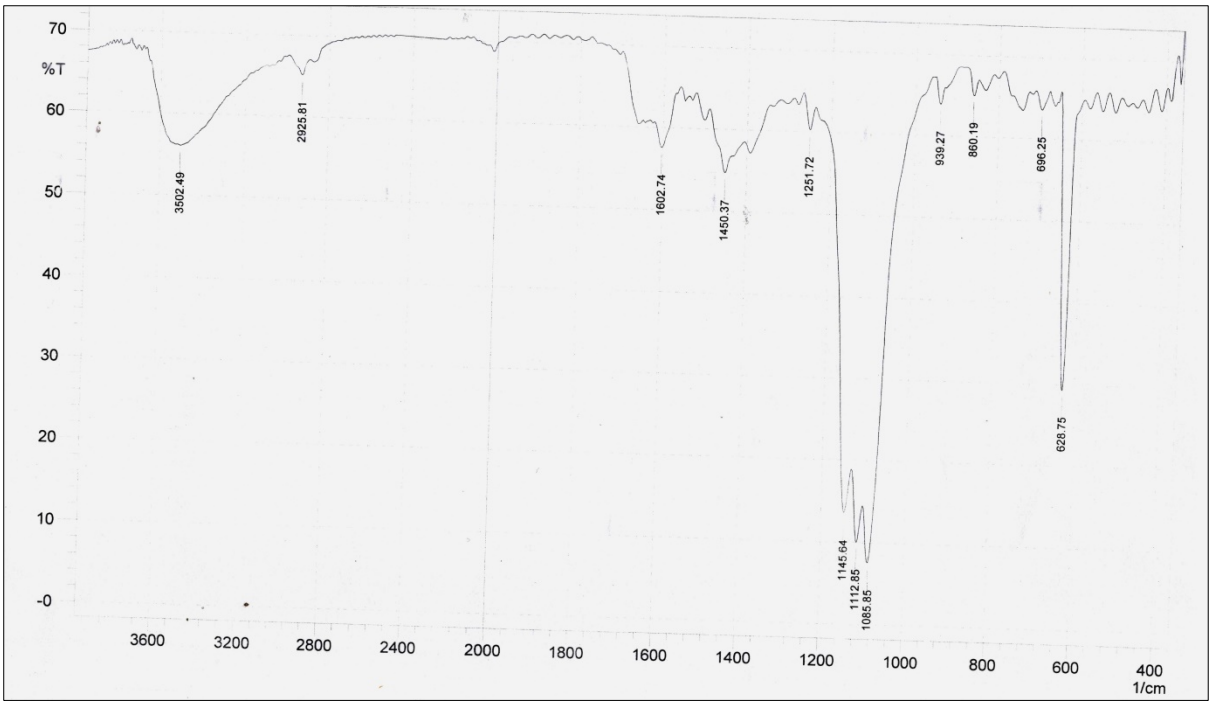

Figure 39S: IR spectrum of **Cd**$^{2+}$-bound **ROTX**.

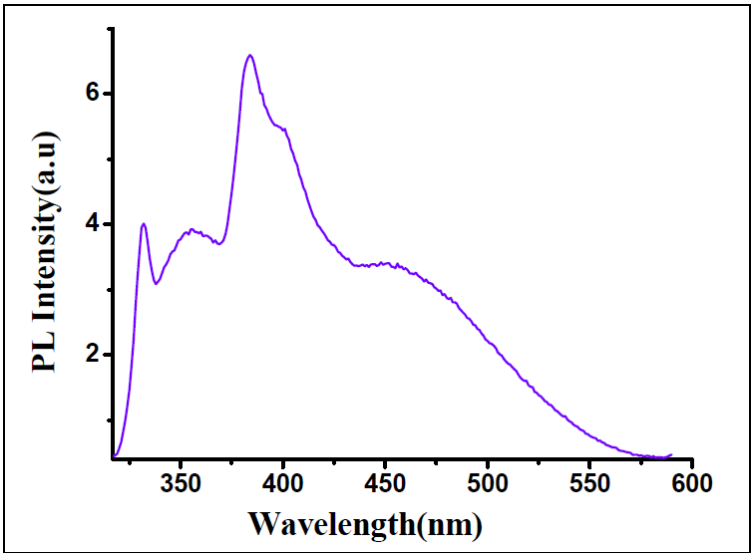

Figure 40S: Characteristic emission spectra of **PYROTX** in dry THF at 298 K, λ_{exc}= 302 nm.

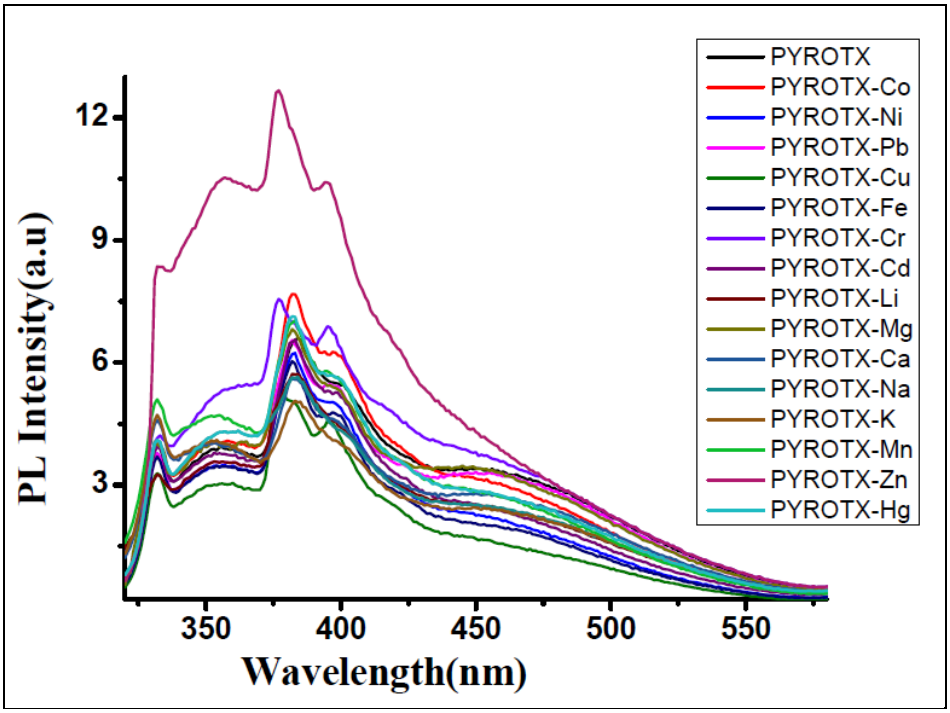

Figure 41S: Emission spectra of **PYROTX** in the presence of 10 equivalents of Ni^{2+}, Cu^{2+}, Mn^{2+}, Cr^{3+}, Co^{2+}, Hg^{2+}, Cd^{2+}, Li^{+}, Na^{+}, K^{+}, Ca^{2+}, Fe^{3+}, $Mg^{2+}$and Pb^{2+} and one equiv. of Zn^{2+} ion in THF at 298 K, λ_{exc}= 302 nm.

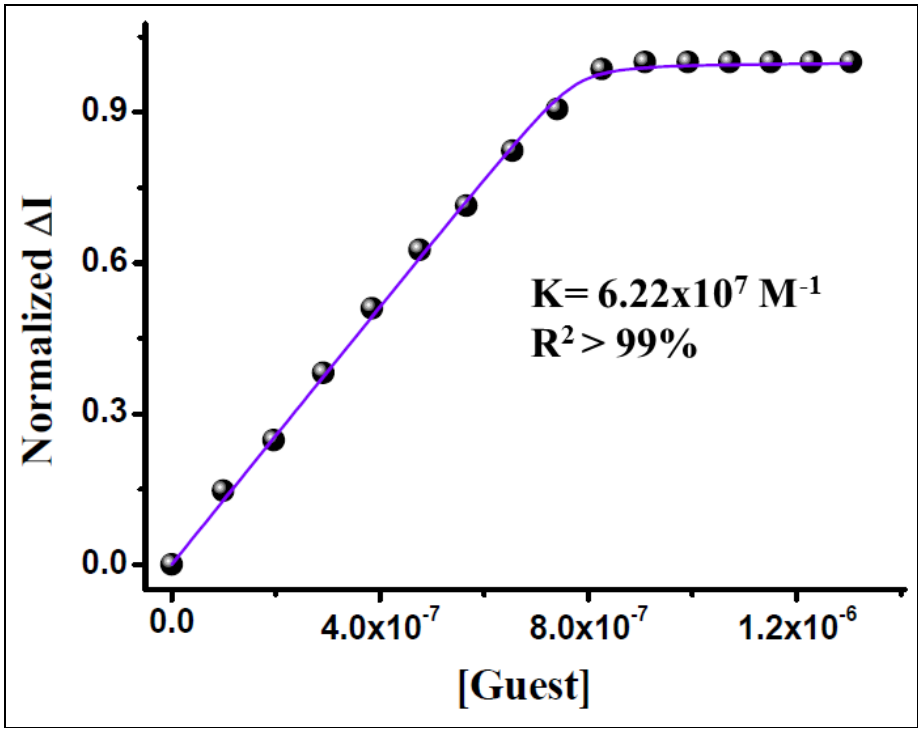

Figure 42S: Non-linear 1 : 1 curve fitting plot from PL titration data between **PYROTX** and Zn^{2+} ion in THF at 298 K, λ_{exc}= 346 nm.

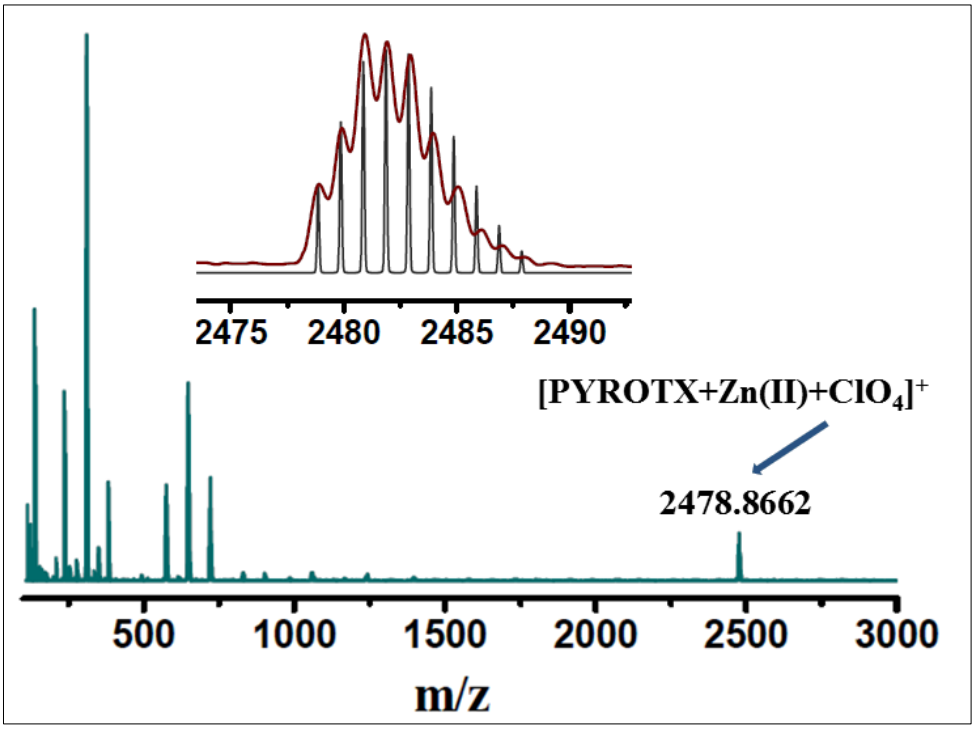

Figure 43S: ESI-MS spectrum of Zn^{2+}-bound **PYROTX**. (Inset picture: isotopic distribution pattern)

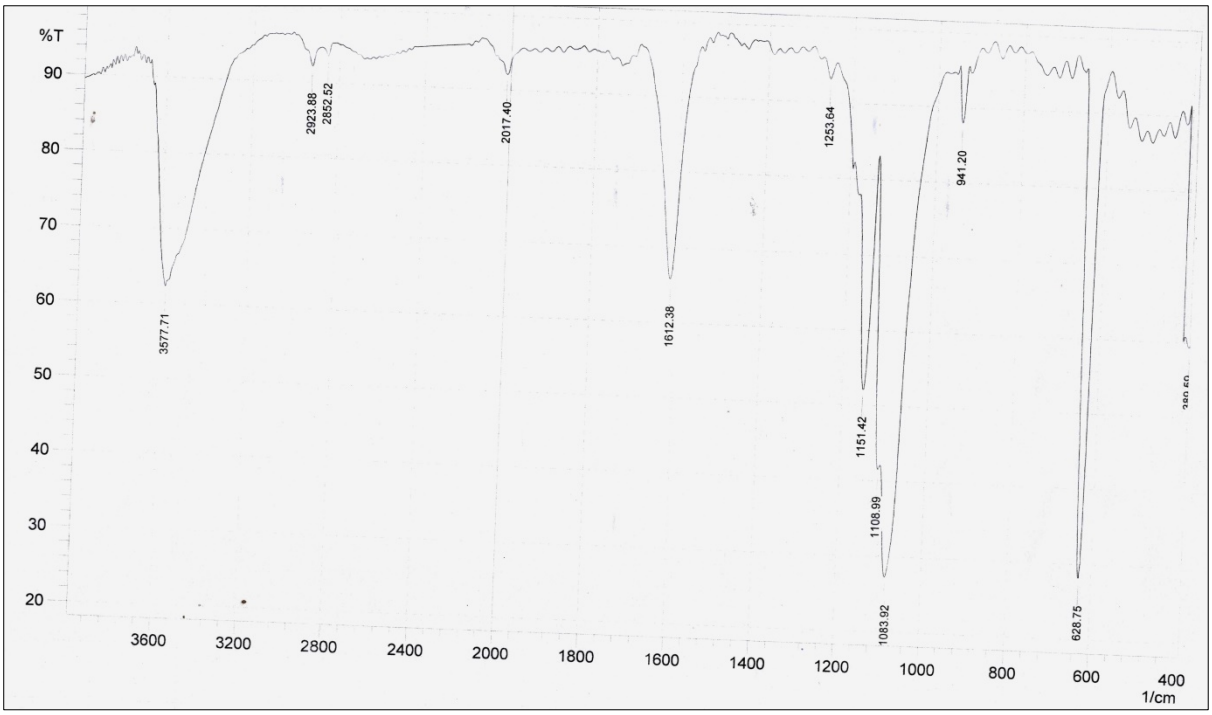

Figure 44S: IR spectrum of Zn^{2+} bound **PYROTX**.

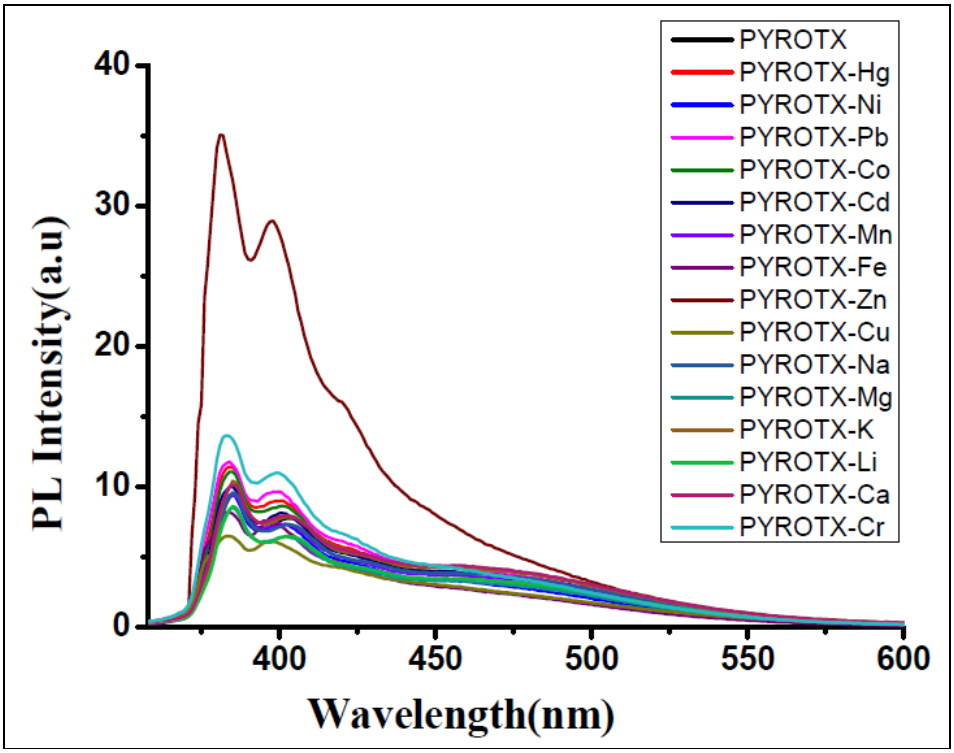

Figure 45S. Emission spectra of **PYROTX** ($1x10^{-6}$ M) in the presence of 10 equivalents of Ni^{2+}, Cu^{2+}, Mn^{2+}, Cr^{3+}, Co^{2+}, Hg^{2+}, Cd^{2+}, Li^{+}, Na^{+}, K^{+}, Ca^{2+}, Fe^{3+}, Mg^{2+}, Pb^{2+} and one equiv. of Zn^{2+}ion in solvent mixture (5% water in THF) at 298 K, λ_{exc}=346 nm.

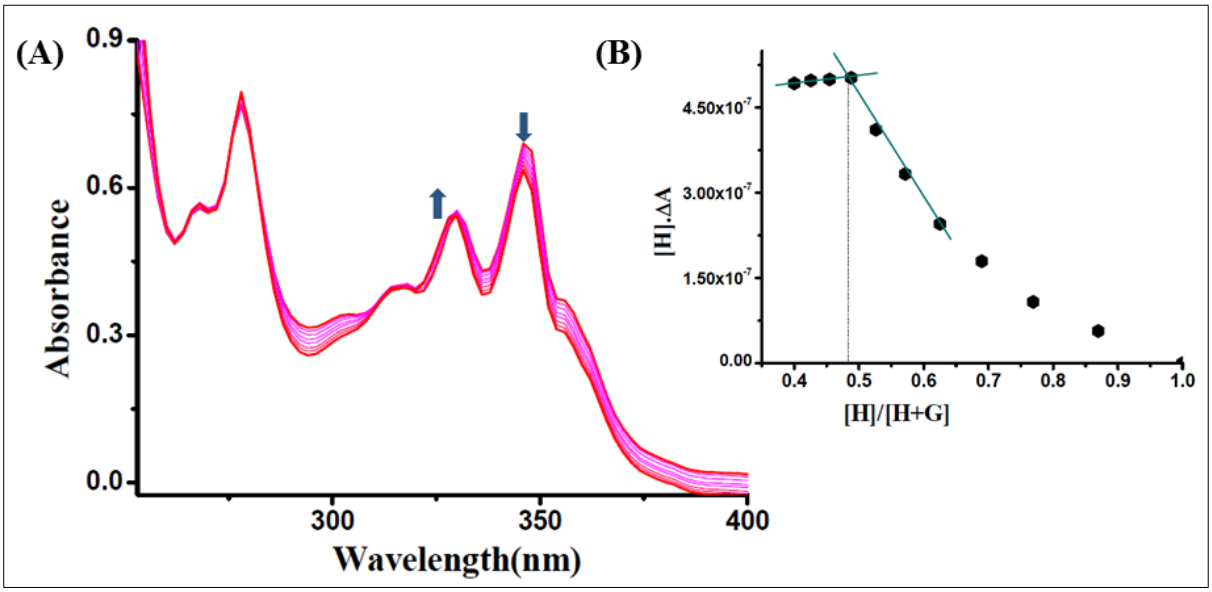

Figure 46S. (A) UV/Vis titration profile of **PYROTX** ($1x10^{-5}$ M) upon addition of Zn^{2+} ($1.15x10^{-4}$ M) in solvent mixture (5% water in THF), (B) molar ratio plot from UV/Vis titration data at 298 K.

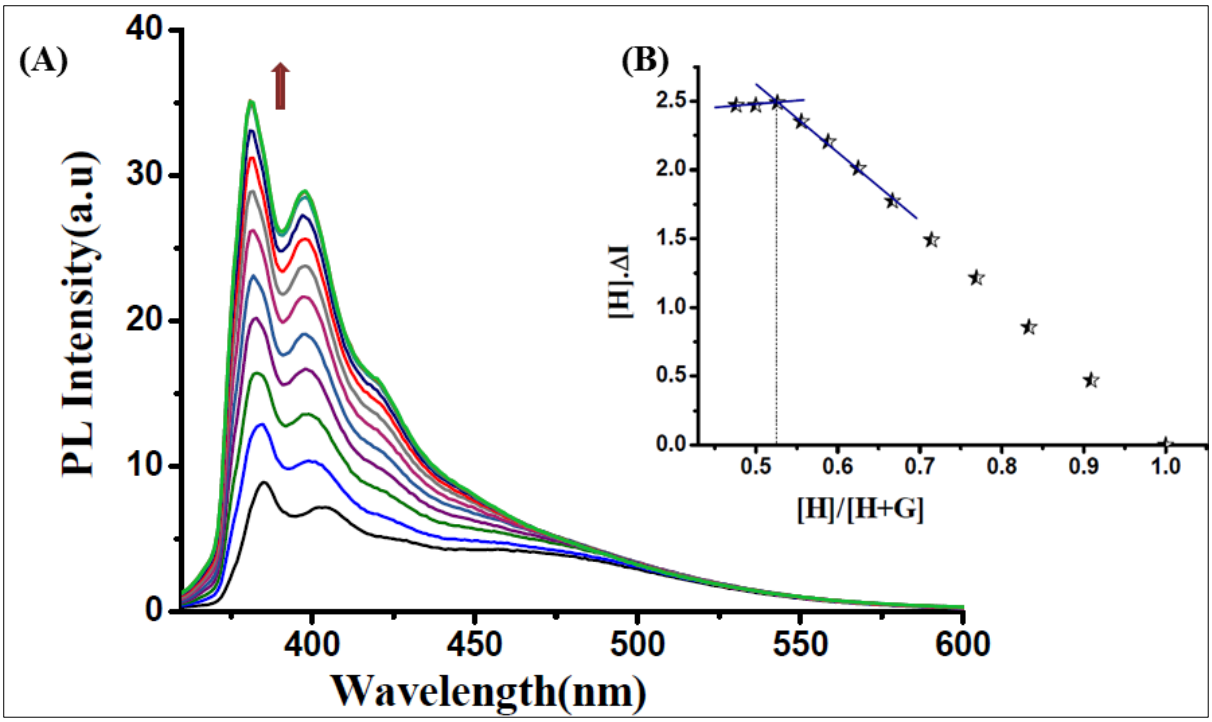

Figure 47S. (A) PL titration profile of **PYROTX** ($1x10^{-6}$ M) upon addition of Zn^{2+} ($1x10^{-5}$ M) in solvent mixture (5% water in THF), (B) molar ratio plot from PL titration data at 298 K.

References:

1. S. Bej and P. Ghosh, *Dalton Trans.*, 2018, **47**, 13408-13418.

2. S. Saha, S. Santra, B. Akhuli and P. Ghosh, *J. Org. Chem.*, 2014, **79**, 11170-11178.

3. S. Bej, M. Nandi, T. K. Ghosh and P. Ghosh, *Dalton Trans.*, 2019, **48**, 6853-6862.